STATISTICS OF SWITCHING-TIME JITTER FOR A TUNNEL DIODE THRESHOLD-CROSSING DETECTOR

DONALD E. NELSEN

TECHNICAL REPORT 456

AUGUST 31, 1967

MASSACHUSETTS INSTITUTE OF TECHNOLOGY

RESEARCH LABORATORY OF ELECTRONICS

CAMBRIDGE, MASSACHUSETTS 02139

MASSACHUSETTS INSTITUTE OF TECHNOLOGY

RESEARCH LABORATORY OF ELECTRONICS

Technical Report 456 August 31, 1967

STATISTICS OF SWITCHING-TIME JITTER FOR A TUNNEL
DIODE THRESHOLD-CROSSING DETECTOR

Donald E. Nelsen

Abstract

As a step toward obtaining a procedure for modeling randomness occurring in electronic switching circuits, the switching randomness, or jitter, arising in a tunnel-diode switch was investigated. Distributions of the switching time were measured for a tunnel-diode switching circuit that was driven by a slowly rising current ramp. A model was deduced from these measurements which relates the statistics of the jitter to the slope of the input ramp, the load resistance, and the tunnel-diode characteristics in the vicinity of the current peak: the amount of shot noise, junction capacitance, and i-v relation curvature. For switching in the reverse direction — from the valley of the i-v relation back to the initial state — the switching randomness involves a different mechanism. Another model is presented for this case. This model relates the jitter to the 1/f noise that predominates in the valley region of the tunnel diode.

TABLE OF CONTENTS

CONTENTS

iv

I. INTRODUCTION

1.1 GENERAL THRESHOLD-CROSSING DETECTION PROBLEM

If a slowly rising ramp is applied to the input of a physical switching circuit, switching will occur when the ramp crosses a threshold level that is characteristic of the circuit. If this switching procedure is repeated a number of times, the observed switching times will be randomly distributed about some mean value. The original objective of this investigation was to determine a method whereby this switching randomness, or jitter, could be related to more fundamental random processes that occur in the devices and elements comprising a particular switching circuit.

The switching circuits for which we would like to model the jitter range from simple single-device circuits, such as the tunnel diode or neon-bulb switches, to more complex regenerative circuits, such as the Schmidt trigger or flip-flop. The numerous applications of these switches include use in sampling systems, switching-type modulators, comparators, and computers.

In many of these applications, operating limitations are imposed by the switching randomness. Hence it would be extremely valuable to be able to evaluate the switching jitter in terms of more fundamental random processes occurring in the elements and devices of a particular switching circuit. With this ability the amount of jitter could not only be predicted for a given circuit, but also reduced or minimized with proper circuit design.

1.2 APPROACH TO THE GENERAL PROBLEM

One would expect, a priori, that jitter in electronic switching circuits arises from random fluctuations associated with the particle nature of the conduction process in the circuit components.

In linear circuits the effects of these fluctuations can be modeled in terms of shot, thermal, and $1/f$ noise descriptions that are well known for most devices and circuit elements that would comprise a particular circuit. It is not clear, however, that the jitter occurring in a switching circuit, which is, of course, highly nonlinear, can be modeled in terms of these specific noise descriptions; in fact, it is conceivable that the jitter could be related only to processes that are more fundamental than the shot, thermal, or $1/f$ noise processes.

A first step toward solving the general problem might be to choose a particular kind of switching circuit and investigate its properties in detail to see if its jitter could be modeled in terms of the shot, thermal, and $1/f$ noise processes that occur in the individual circuit components. If such a model could be determined for that one kind of switch, then it is likely that the same modeling procedure could be used for other kinds of switching circuits.

Even if this approach were not successful, valuable insight into the switching process

1

would have been gained, and a definite contribution would have been made in showing that the jitter is probably caused by processes more fundamental than the shot, thermal, or 1/f noise processes.

The thesis research was concerned with this initial approach to the general threshold-crossing detection problem. The tunnel diode switch was chosen for this initial investigation for the following reasons: the circuitry of the switch is simple; the tunnel diode's noise model is relatively simple and is valid over an extremely wide frequency range (of all electronic devices in existence today, the tunnel diode has one of the widest bandwidths); and diodes with characteristics matched within a few per cent can be easily obtained. The last property is important, since a differential technique was used for measuring the statistics of the jitter.

1.3 RESEARCH OBJECTIVE

The object of the present investigation was to determine the mechanism whereby switching jitter arises in the tunnel diode switch. First, relationships between certain statistics of the jitter and various circuit and device parameters were measured experimentally. Then, with the insight obtained from these observations, a model was determined that relates the statistics of the switching randomness to certain circuit parameters and to the shot, thermal, and 1/f noise formulations of the tunnel diode model. Finally, additional experiments suggested by the theoretical results were performed to check the range of applicability of the model.

II. REVIEW OF BASIC TUNNEL-DIODE SWITCHING OPERATION
AND NOISE CHARACTERISTICS

A literature search revealed that previous investigations pertinent to our present problem dealt either with models for describing the noise behavior of tunnel diodes in linear circuits or with nonrandom models describing deterministic switching behavior of tunnel diodes. The model that will be developed in this report is based on notions in each of these areas. This section reviews basic operation of a tunnel diode switch and presents a commonly accepted noise model of the tunnel diode. A discussion of basic tunnel diode characteristics will provide insight that will be helpful in understanding the nature of our problem and its solution.

2.1 BASIC SWITCHING OPERATION

a. Definitions of Switching in the "Forward" and "Reverse" Directions

If the circuit shown in Fig. 1, consisting of a load resistor, R_L, in parallel with a tunnel diode, is excited by a current ramp, $\alpha t u_{-1}(t)$, as shown in Fig. 2, the operating
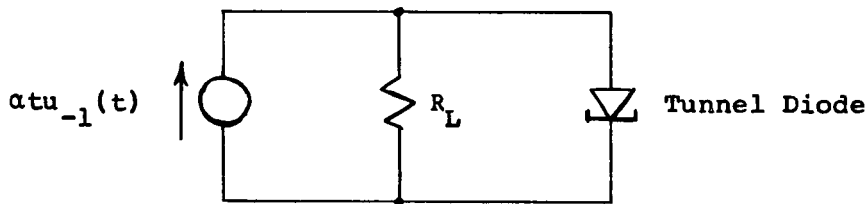
Fig. 1. Basic form of the tunnel diode switching circuit.
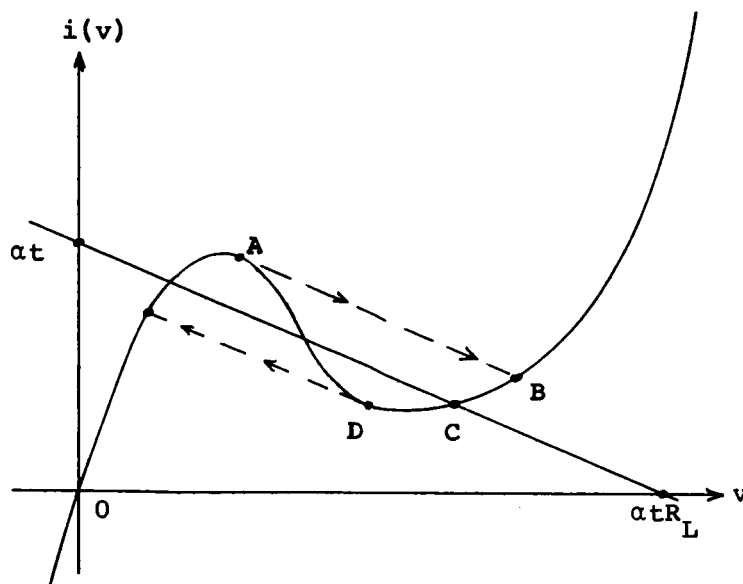
Fig. 2. Tunnel diode static i-v characteristic, showing the path of the operating point during switching.

3

point will travel from the origin along the i-v curve as shown in Fig. 3. When the operating point reaches the peak of the characteristic (at A in Fig. 3), switching will occur as it jumps to the other stable state at B in the figure. We shall call this switching, from the peak across the valley to the other state, <u>forward-direction switching.</u>

If the input current were then decreased, the operating point would travel from B until it reached C, where the load line is tangent to the diode characteristic. Then the diode would switch back to the original state as the operating point jumps to D. This switching will be called <u>reverse-direction switching</u>.

b. Occurrence of Switching-Time Randomness, or Jitter

If either of the two switching operations described above were to be repeated a number of times under identical conditions, we would find that the observed switching times are randomly distributed about some mean. This randomness, or "jitter," of the switching times arises because of the random fluctuations associated with the quantized nature of the conduction process.

It is our purpose here to relate the statistics of the jitter to more fundamental descriptions of the particle fluctuations. Such descriptions are the shot, thermal and 1/f noise formulations.

2.2 A NOISE MODEL FOR THE TUNNEL DIODE

In order to gain more insight into the nature of this switching problem, we shall present a commonly accepted model for the tunnel diode.[1-3] This model, derivable from the basic physics of the device, is shown in Fig. 3. Although the model is normally used to describe linear operation of the diode, it will be helpful now in providing insight into the mechanism of coupling between particle randomness and switching jitter. In Section IV this model will be used to relate the switching-time statistics to more fundamental circuit and device parameters.

Series resistance and inductance of the leads are neglected in this model. The familiar static i-v characteristic i(v) shown in Fig. 2, is considered here to be instantaneous, or memoryless.
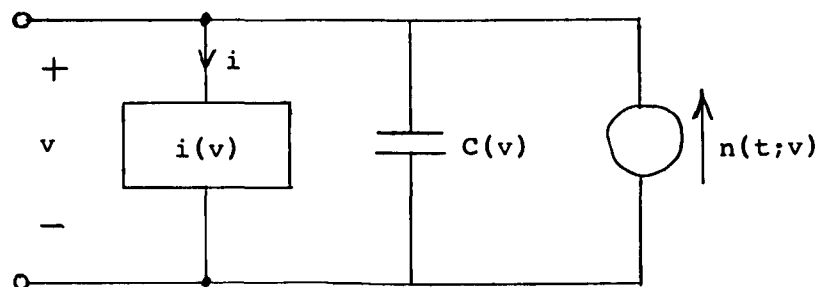
Fig. 3. Equivalent circuit model of the tunnel diode.

The junction capacitance, $C(v)$, is a function of voltage. It is linearized capacitance, valid for small-signal operation about an operating point at v volts. $C(v)$ can be used for larger signals, too, without very much loss in accuracy, since its value is not strongly dependent upon v in the switching region.

The characteristics of the noise, $n(t;v)$, depend strongly on the operating voltage v. Noise of two basic types has been measured in tunnel diodes. One variety is white, at least up to the diode cutoff frequency, and has been very well accounted for by using a shot-noise model. The other type is present predominantly at low frequencies and has approximately a $1/f$ variation in spectral height. These two types of noise will now be discussed in more detail.

a. Shot Noise in Tunnel Diodes

The shot and $1/f$ noises predominate in different operating regions of the diode: shot-noise predominates in the vicinity of the peak of the i-v relation; $1/f$ noise, in the valley.

The voltage dependence of the shot noise has been studied theoretically and experimentally by Berglund, Pucel, and Turner and Burgess.[1-3] We shall summarize their results.

If a current I_1 that is generated by a single source is flowing across a semiconductor junction, the shot noise caused by the corpuscular nature of the current flow will have a two-sided, white, power density spectrum of height eI_1, where e is the magnitude of the electron charge.

In the tunnel diode, however, there are two components of current simultaneously flowing in opposite directions across the junctions. These components of current are generated by independent processes. The first component is the Esaki, or tunneling current, I_E, and the second is the Zener current, I_Z. The net terminal current of the diode is given by the difference between these components,

$$i = I_E - I_Z. \tag{1}$$

Each component contributes its own shot noise. Thus the resulting total noise will be the sum of the two noise components. Since the two noise components are independent, the two-sided spectrum, $S(f)$, of the total noise will be the sum of the spectra of the separate components. That is,

$$S(f) = e\left(|I_E| + |I_Z|\right) = eI_{eq}. \tag{2}$$

In this expression the equivalent shot-noise-producing current, I_{eq}, is

$$I_{eq} = |I_E| + |I_Z|. \tag{3}$$

This current, I_{eq}, is different from the terminal current i, given in Eq. 1 if I_E and I_Z are both nonzero. In Fig. 4 the currents I_E, I_Z, i, and I_{eq} are plotted as a

$$i(v), \quad I_{eq}(v), \quad I_E(v), \quad I_Z(v)$$

$$I_{eq}(v) = \left| I_E(v) \right| + \left| I_Z(v) \right|$$
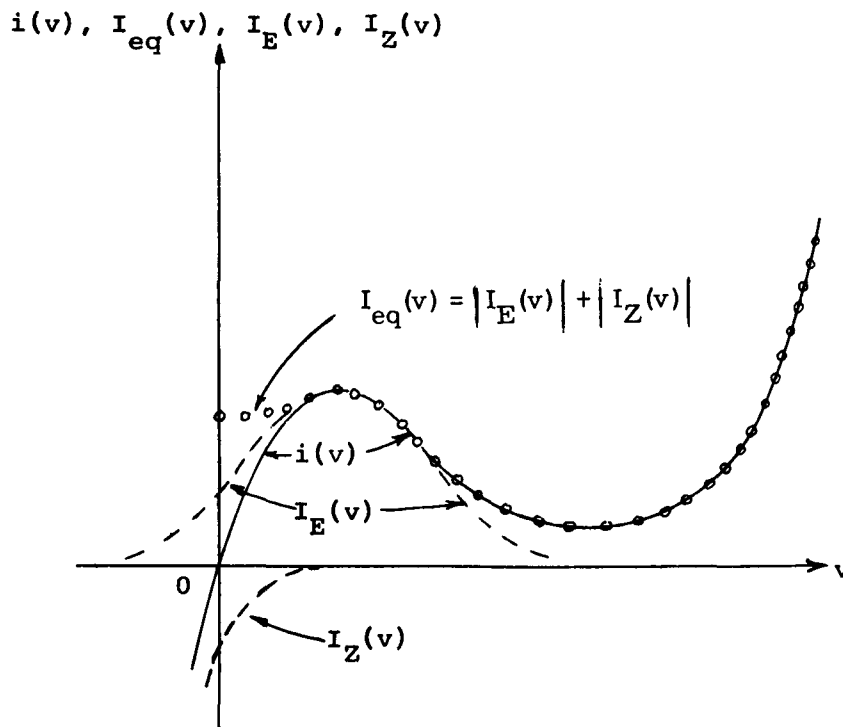
Fig. 4. Relation between actual current, $i(v)$, and the equivalent shot current, $I_{eq}(v)$.

function of voltage v. It is significant that in the region near the peak of $i(v)$,

$$I_{eq}(v) \cong i(v). \tag{4}$$

It will be shown, for forward switching, that the noise affects the switching randomness most strongly in the region near the peak of $i(v)$. Thus Eq. 4 will be a useful simplification for our modeling of the jitter mechanism.

b. 1/f Noise in the Tunnel Diode

In contrast to shot and thermal noises, which have well understood models, the physical origin of 1/f noise has not, as far as we know, been explained. 1/f noise, characterized by the 1/f variation of its power spectrum, is observed almost universally in materials.

A number of experimental investigations of 1/f noise in tunnel diodes have been performed. Yajima and Esaki[4] were not able to detect any significant 1/f noise in the peak and negative-resistance regions of germanium tunnel diodes. When, however, the diode voltage was increased beyond the negative-resistance area into the valley region, a marked increase in 1/f noise was observed. For instance, the 1/f noise level that they measured at 1 kc in the valley region was greater than the shot-noise level by a factor of approximately 10^4.

Berglund[1] in his experimental study claims that the 1/f noise in the valley region

6

may predominate over shot noise up to frequencies as high as 50 Mc.

The following properties of tunnel diode noise will be important in the modeling of switching-time randomness: (a) in the peak region of the tunnel diode, shot noise is the dominant form of noise; (b) in the diode's valley region, the 1/f noise is dominant.

2.3 DIFFERENCE EXPECTED BETWEEN FORWARD AND REVERSE SWITCHING

In terms of the noise model just discussed above, we shall now try to gain insight into a mechanism whereby the noise affects the switching-time randomness. It is not clear at this point that the switching randomness can be related to the specific shot or 1/f noise processes just described; it is entirely possible that the jitter can only be related to random processes that are more fundamental than those observed in the small-signal noise model. (In the models developed later in this report, however, we are able to relate the switching randomness to the shot and 1/f noises.)

For each of the two switching directions it is possible to define a critical operating region where coupling between particle randomness (or noise) and jitter is likely to be most important.

For forward switching, the "decision" to switch is made in the circuit when the operating point is near the peak of the i-v curve, just before its jumping to the other state. If the operating point has not yet reached this peak region, noise fluctuations are not likely to influence the time of switching. On the other hand, if the operating point is already past this critical coupling area, the diode is already well on its way toward switching, and will be negligibly influenced by the noise. Thus the noise will have the strongest effect on the switching time in a relatively small region near the peak of the i-v curve.

By using similar reasoning, it can be concluded that the corresponding critical coupling region for reverse-direction switching is in the valley region, near the point of tangency between the load line and the i-v curve.

By examining the linear noise model just presented, the important observation that different types of noise exist in the respective critical coupling regions for forward and reverse switching can be made.

White shot noise predominates in the critical region for forward switching near the current peak whereas low-frequency 1/f noise dominates in the reverse-switching critical region in the valley of the i-v relation. Thus we would expect that the switching randomness observed for the two switching directions would be different.

This is indeed the case. The experimentally determined jitter behavior for forward switching was different from that observed for reverse switching. Separate models will be developed for the respective switching directions. Greater emphasis will be placed in this report on forward switching, since forward switching is faster, and hence more commonly used than reverse switching. A separate section on reverse-direction switching will be included in Section V.

7

III. EXPERIMENTAL DETERMINATION OF SWITCHING-TIME STATISTICS

At the outset of this investigation the only information we had concerning the mechanism whereby jitter might arise in a tunnel diode switch was that which could be deduced from the linear noise model presented in Section II. In order to gain more insight into the jitter process, we decided to measure the switching-time distribution as a function of slope of the input ramp and other circuit parameters. With this additional information, we hoped to be able to construct an adequate model of the process.

We shall describe here the basic experiment, discuss techniques that were used, and present the more important experimental results. Some additional experiments that were suggested by the theoretical results are included in Section V. A summary of experimental and theoretical results will be presented in Section VI. Detailed circuit diagrams corresponding to the measurement techniques are included in the appendices.

Measurements described here will be for forward-direction switching only. Experiments concerning reverse-direction switching will be presented in Section V, since an entirely different theory describes those results.

3.1 BASIC EXPERIMENT

The basic experiment consisted of generating a voltage ramp of slope a, applying this to a tunnel diode in series with the load R_L, and then measuring the random switching time T_S. This experiment was repeated enough times to yield reasonable statistical accuracy in estimating the switching-time distribution. Distributions were measured as a function of input slope a and load resistance R_L.

3.2 MEASUREMENT TECHNIQUE

a. Ramp Generator and Differential Switching Circuit

The basic switching circuit, including the ramp generator and tunnel diode switches, is shown in Fig. 5. To obtain sufficient measurement accuracy, a differential technique was used. This technique will be discussed in more detail below.

The input ramp is generated by the charging of an R-C circuit. If the switch S (in Fig. 5) is opened at t = 0, the rising exponential, $v_s(t)$, shown in Fig. 6, results.

When the ramp reaches the threshold level, V_{T1}, the first diode switches at time T_{S1}. A short time later, the second diode switches at time T_{S2}. The range over which the switching times T_{S1} and T_{S2} vary is small enough to ensure that the rising exponential appears as a constant-slope ramp at the switching levels of both diodes.

The time difference, $T_{S2} - T_{S1}$, is measured by subsequent circuitry. By repeating the experiment many times, the distribution of the difference $T_{S2} - T_{S1}$ is obtained.

The switch S is actually a transistor that is driven by a square-wave generator, which causes the experiment to be repeated periodically. A detailed schematic of the generator and switching circuits is presented in Appendix A.
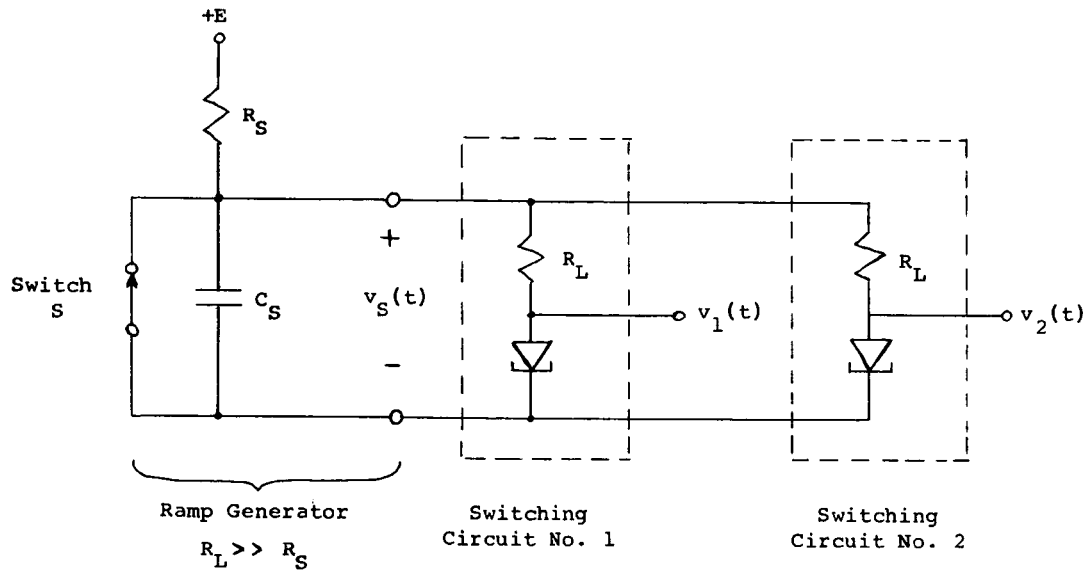
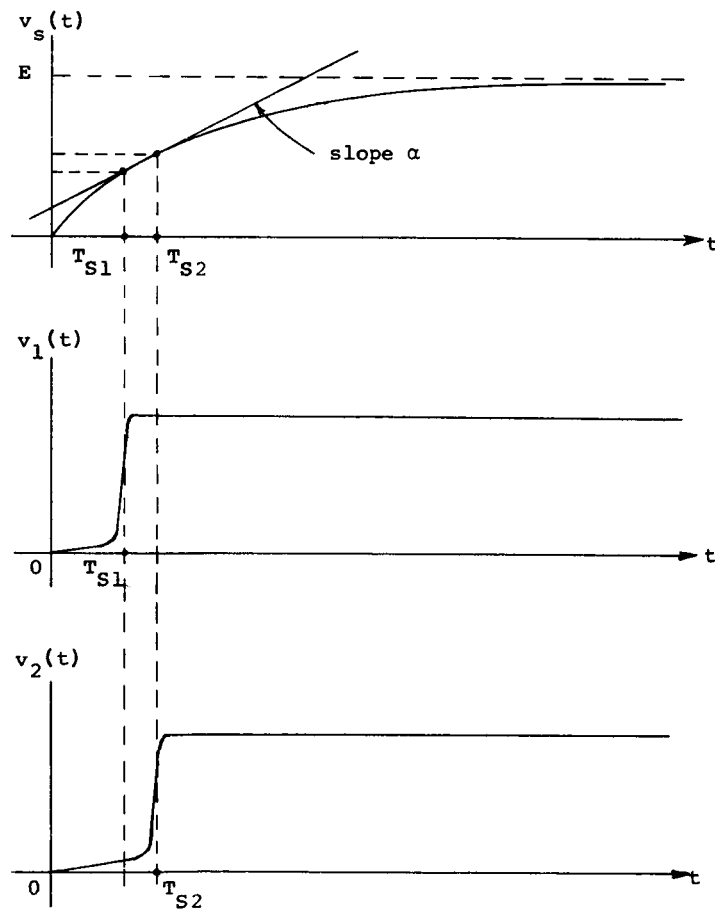Fig. 5. Circuit for differential measurement of jitter.

Fig. 6. Switching waveforms corresponding to the differential circuit of Fig. 5.

b. Differential Measurement Technique

To obtain suitable accuracy, a differential technique was used, since the range of the switching-time randomness is extremely small compared with the interval from $t = 0$ to $t = T_S$. Typically, T_S was 5 msec, while the jitter standard deviation was 5 nsec. Consequently, a measurement accuracy of one part in 10^6 would have been required for direct measurement of the standard deviation. With the differential technique the typical accuracy requirement was one part in ten.

<div align="center">

Statistical Information Obtainable by Using the
Differential Measurement Method

</div>

Because the data obtained by using the differential measurement scheme involve only the switching-time difference, $T_{S2} - T_{S1}$, certain information concerning the statistics of the individual random variables, T_{S1} and T_{S2}, will be lost. Nevertheless, if the two diode circuits switch independently and have identical statistical characteristics, much information concerning the statistics of the separate random variables, T_{S1} and T_{S2}, can be inferred.

The variance of a sum of two statistically independent random variables is equal to the sum of the variances of the separate variables. If the random variables, T_{S1} and T_{S2}, are independent and have the same statistics, then the variance corresponding to either T_{S1} or T_{S2} is half the variance of the difference, $T_{S2} - T_{S1}$.

It is well known that the distribution of a sum of two statistically independent random variables is the convolution of the distribution of one with that of the other. Since we are looking at the difference between two independent random variables, T_{S1} and T_{S2}, that have the same distribution, the distribution of the difference, $T_{S2} - T_{S1}$, will be the autocorrelation of either T_{S1} or T_{S2}.

Specific information can be gained concerning the separate distributions of T_{S1} and T_{S2} if the difference, $T_{S2} - T_{S1}$, is observed to be Gaussian (as was the case).

Cramér[5] proved the following theorem originally conjectured by Lévy: "If the sum of two independent random variables is normally distributed, then each variable is itself normally distributed." The proof of this theorem is quite involved. The theorem provides a necessary link in interpretating the experimental results that were obtained.

It is significant that all information concerning the individual mean switching times, $\overline{T_{S1}}$ and $\overline{T_{S2}}$, is lost due to subtraction that occurs in the difference measurement.

The model derived in the next chapter completely predicts the switching time distribution as a function of circuit parameters and input slope. Using the differential method, we shall be able to check the predicted distribution shape and variance experimentally as a function of circuit parameters. We will not be able to experimentally verify the theoretical predictions concerning the mean due to the differential technique.

c.   Measurement of Statistics of the Switching-Time Difference, $T_{S2} - T_{S1}$

The circuit just discussed yields switching-time difference, $T_{S2} - T_{S1}$. Two methods

that were used for measuring statistical properties of this difference will now be discussed.

The first method was more direct, yielding the complete distribution of $T_{S2} - T_{S1}$. Once the shape of the distribution of $T_{S2} - T_{S1}$ had been determined, a second, more convenient, method was used for further investigation of the jitter statistics. This second measurement method yielded the variance of $T_{S2} - T_{S1}$.

Method I: Measurement by Using a Pulse-Height Analyzer

A block diagram of the system used for directly measuring the distribution of the switching-time difference, $T_{S2} - T_{S1}$, is shown in Fig. 7.
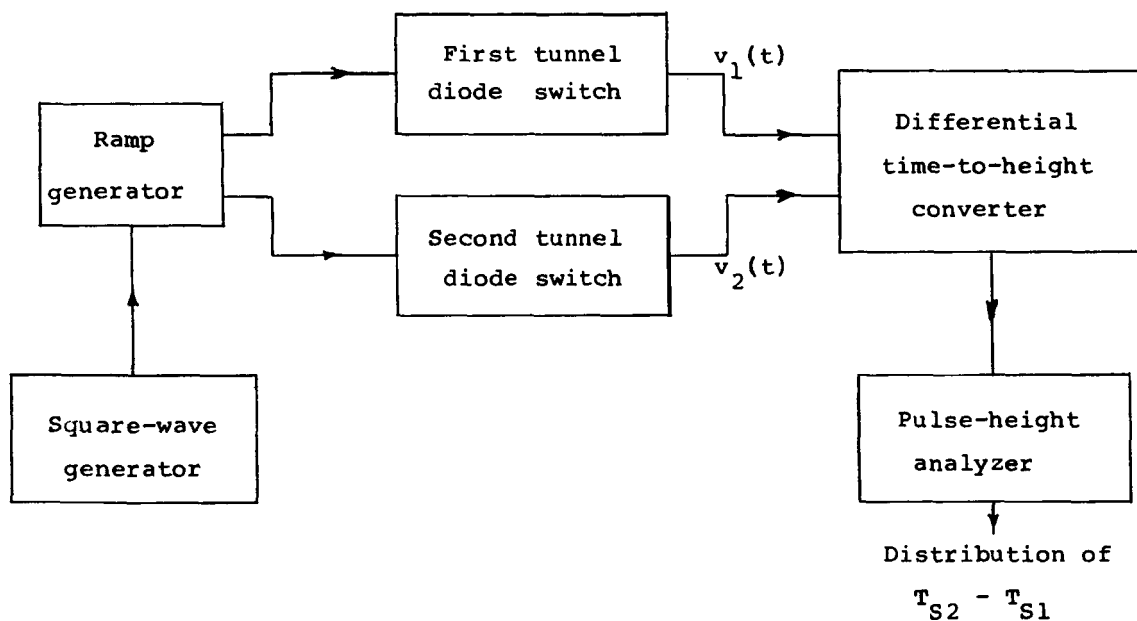
Fig. 7. A system for measuring jitter distribution by means of a pulse-height analyzer.

The voltages $v_1(t)$ and $v_2(t)$, shown in Figs. 5 and 6 are applied to a differential time-to-height convertor (a system that produces an exponential pulse of height proportional to the difference $T_{S2} - T_{S1}$).

After both diodes switch (and the above-described pulse is formed), the ramp is set back to zero, thereby causing the diodes to revert to their original states. The experiment is then repeated, thereby causing both diodes to switch again and another pulse, proportional to the new switching-time difference, to be formed. This procedure is repeated periodically, generating a train of pulses that have random amplitudes, each proportional to the difference $T_{S2} - T_{S1}$ obtained for its respective experiment.

This train of pulses of random heights is then applied to a 400-channel pulse-height analyzer. The analyzer automatically forms the distribution of the amplitudes of the

ensemble of pulses. The distribution of $T_{S2} - T_{S1}$ thus obtained is then read out digitally in channel increments of 2.2 nsec. Between 10,000 and 100,000 pulses were typically observed for each distribution.

The over-all measuring system was very linear. The total error introduced by the system was much less than the 2.2-nsec channel width.

The pulse-height analyzer has 400 memory channels and a magnetic core memory that can store up to 10^5 events in each channel. The analyzer (Model 34-12) was manufactured by the Radiation Instrument Development Laboratory.

A distribution that was being measured could be monitored on an oscilloscope as it was forming. Thus the convergence of the distribution could be observed, and the measurement stopped when the statistical error, which was due to the limited sample size, became small enough.

The digital output could either be printed, plotted automatically, or punched onto paper tape for further processing.

Method II: Measurement of the Variance of the Difference $T_{S2} - T_{S1}$ by Using a Spectral Method

This second, less direct, method of measuring $T_{S2} - T_{S1}$ was used, once the shape of the distributions had been determined. This method was more convenient than the first, since it could be implemented by using equipment that was available in our own laboratory.

As in Method I, a periodic train of pulses having random amplitudes proportional to the values of $T_{S2} - T_{S1}$ obtained in the respective repeated experiments was generated. This train is shown in Fig. 8a.

A property of the power density spectrum of this random pulse train was utilized in order to obtain an estimate of the variance of $T_{S2} - T_{S1}$. The power density spectrum, S(f), of this random pulse train is shown in Fig. 8b, and is derived in Appendix B. We assumed that the respective pulse heights were uncorrelated, that is, that switching-time differences corresponding to different experiments were uncorrelated.

As shown in Fig. 8, the spectrum consists of continuous and impulsive components. These components correspond to the random and periodic components of the random pulse train, respectively.

The important characteristic of the spectrum S(f) is that its continuous part is proportional to the variance (which is what we desire) of the amplitudes of the respective pulses.

If the random heights are denoted by the random variables, x, having the variance σ_x^2, then the spectrum of the continuous part of the spectrum, $S_r(f)$, is

$$S_r(f) = \frac{\sigma_x^2 \tau^2}{T} \frac{1}{1 + (2\pi f \tau)^2},$$ (5)

$$\frac{\sigma_x^2 \tau^2}{1 + (2\pi f \tau)^2}$$
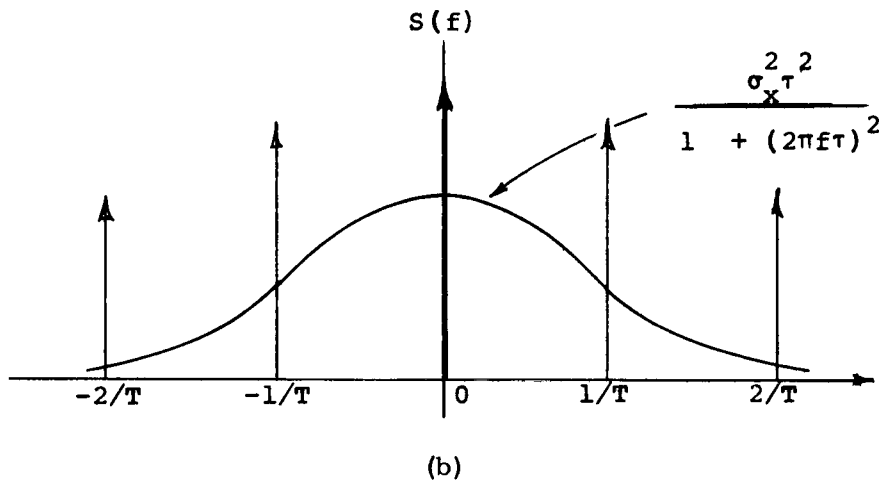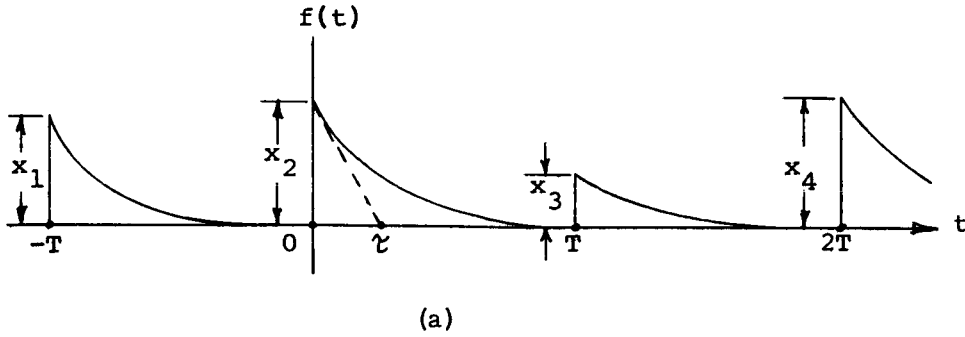
Fig. 8. (a) Periodic train of random-amplitude pulses obtained in the measurement process. The random amplitudes x_1, x_2, x_3, ... are proportional to the values of $T_{S2} - T_{S1}$ obtained in the respective experiments.
(b) Power density spectrum $S(f)$ of $f(t)$.

where τ is the time constant of the exponential, and T is the period of the pulse train.

Consequently, by passing the pulse train through a bandpass filter that passes some of the continuous part of the spectrum and rejects the impulses at harmonics of $1/T$, an output signal with mean-square value proportional to the variance σ_x^2, or equivalently the variance of $T_{S2} - T_{S1}$, is obtained.

A block diagram of the over-all system that was used for accomplishing this processing is shown in Fig. 9.

We might mention here that we assumed in the derivation that the pulse amplitudes were mutually uncorrelated. For forward-direction switching, when the main source of jitter is from shot noise (effectively white) one would expect this assumption to be valid. For switching in the reverse direction, however, where $1/f$ noise

13

```
                    ┌─────────────────┐
                    │  First tunnel   │
                    │  diode switch   │──── $v_1(t)$ ──┐
                    └─────────────────┘                │    ┌──────────────────┐
┌──────────────┐                                       └───▶│   Differential   │
│     Ramp     │────────┐                                   │  time-to-height  │
│   generator  │────┐   │  ┌─────────────────┐              │    converter     │
└──────┬───────┘    └──▶│  Second tunnel   │               └────────┬─────────┘
       │               │  diode  switch   │──── $v_2(t)$ ──┘        │
       │               └─────────────────┘                ┌─────────▼────────┐
┌──────┴───────┐                                          │    Bandpass      │
│  Square-wave │                                          │     filter       │
│   generator  │                                          └─────────┬────────┘
└──────────────┘                                          ┌─────────▼────────┐
                                                          │  True rms meter  │
                                                          └─────────┬────────┘
                                                                    │
                                                          Variance   of
                                                          $T_{S2} - T_{S1}$
```
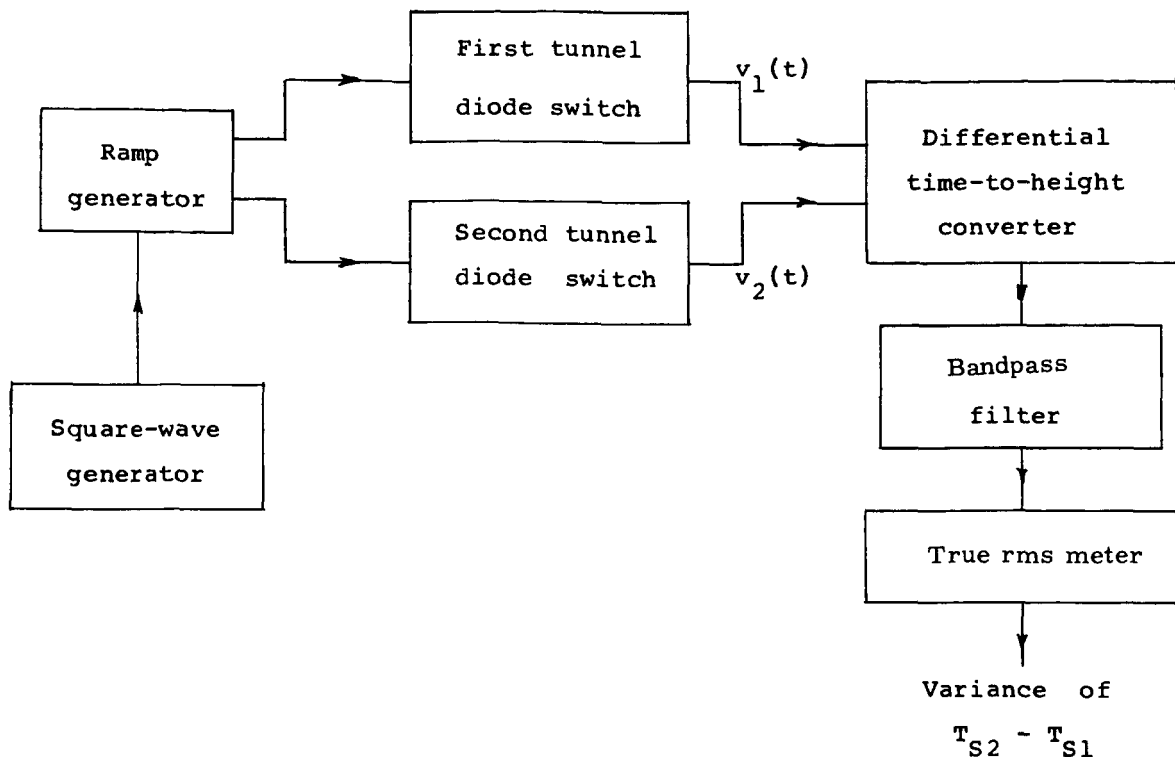
Fig. 9. Block diagram of the system used for measuring the variance of $T_{S2} - T_{S1}$ by means of the spectral method.

is the main cause of jitter, the switching times corresponding to successive experiments are highly correlated. Consequently, this spectral measurement method just discussed is not directly applicable in the reverse-switching case. We checked the validity of the forward-switching results obtained by this method by comparing them with those obtained by using the direct procedure of Method I.

3.3 EXPERIMENTAL RESULTS

The most important experimental results — those that were useful in deriving the theoretical model to be presented in Section IV — will be presented here. Results of other experiments that were motivated by predictions of the model will be presented in Section V. Since these results are somewhat scattered throughout this report, they will all be summarized in Section VI.

Germanium, 1-ma tunnel diodes (G. E. Type 1N3713) were used for the results reported here.

a. Jitter Distribution

The measured distributions of the switching-time difference, $T_{S2} - T_{S1}$, were Gaussian within the statistical accuracy obtainable with the limited sample size. A

typical distribution is shown in Fig. 10. A plot of this distribution on probability paper is shown in Fig. 11. The curve is extremely linear in the central region, which indicates that the curve is essentially normal there. The deviation in the tails is statistical variation that is to be expected, since the number of points in the tails is much smaller than the number in the central region.
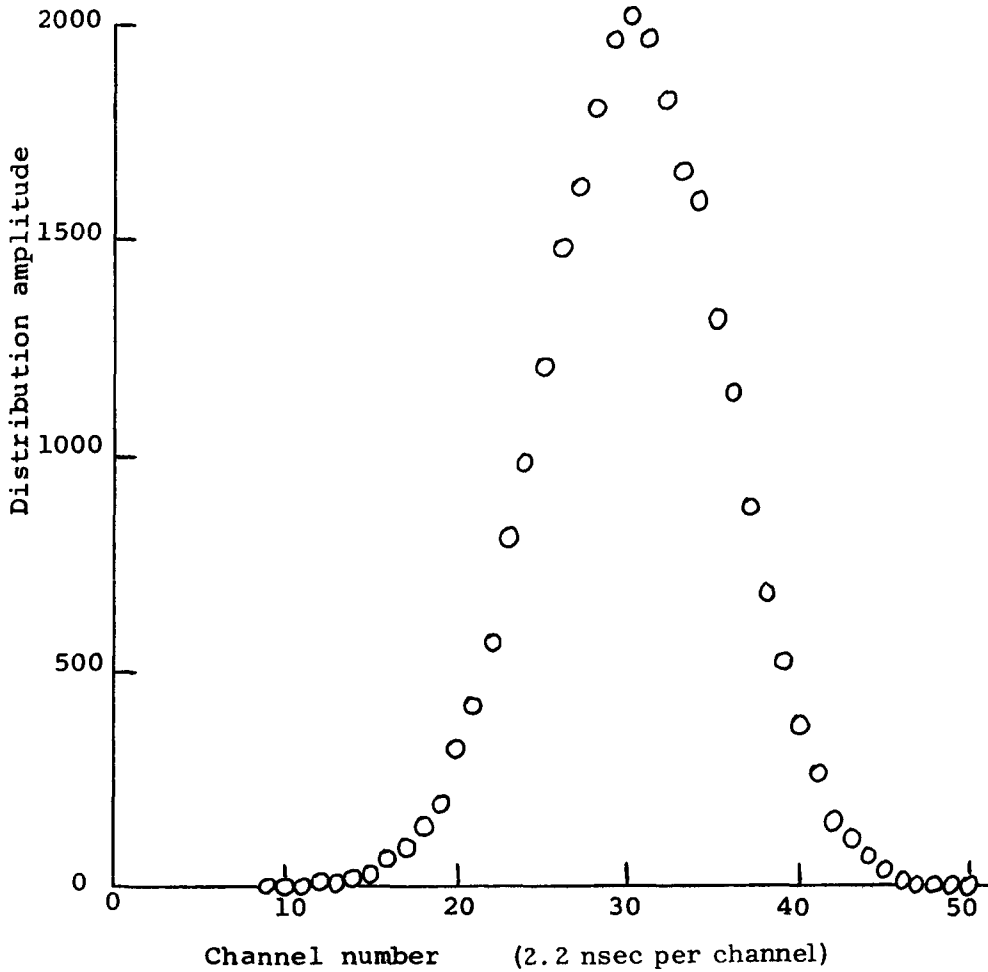
Fig. 10. Typical distribution of $T_{S2} - T_{S1}$, measured for $R_L = 4$ kΩ and slope $a = 5.01$ amps/sec. Number of samples: 26,600.

Jitter distributions were measured for a variety of values of input slope a and load resistance R_L, and in all cases, were Gaussian.

By the Cramér-Lévy theorem discussed above, the separate distributions of T_{S1} and T_{S2} are Gaussian if the difference, $T_{S2} - T_{S1}$, is Gaussian. Thus, since the measured distribution of $T_{S2} - T_{S1}$ is Gaussian, the separate random variables are Gaussian.

15
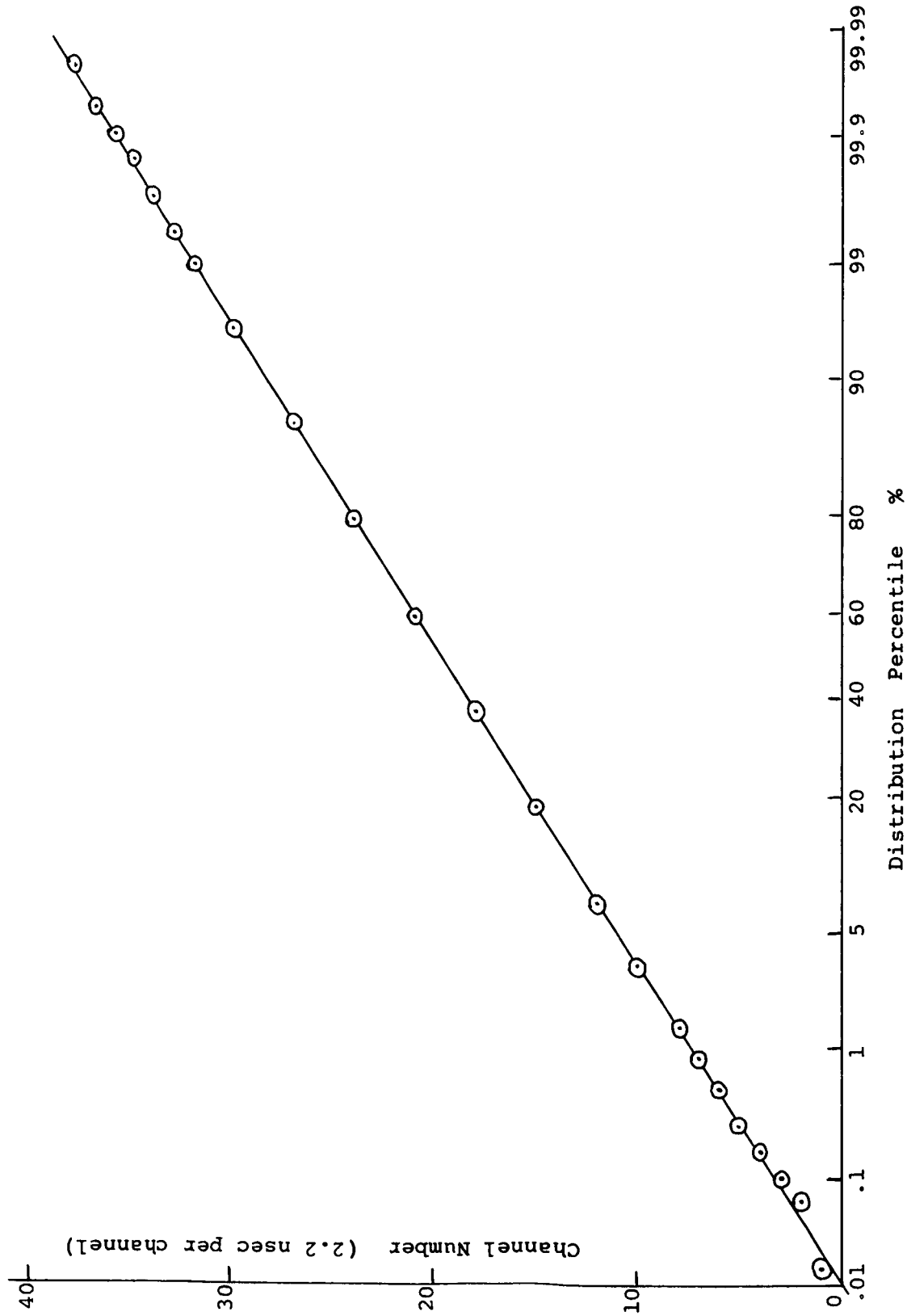
Fig. 11. Plot of integrated probability distribution of $T_{S2} - T_{S1}$ on probability paper. Measuring Conditions: $R_L = 4 \ k\Omega$; slope $a = 5.01$ amps/sec; number of samples = 22, 600.

b.   Jitter Standard Deviation, σ_T, as a Function of Slope, a

A typical plot of σ_T versus a for R_L = 4 kΩ is shown in Fig. 12. Measurement of the relation between σ_T and a was made for several different values of load resistance, R_L. In all cases, the observed dependence could be approximated, within the typical accuracy shown in Fig. 12, by

$$\sigma_T \sim \frac{1}{a^p},$$
(6)

where 0.77 < p < 0.85. The value of p depends upon the specific pair of diodes used and only slightly upon the value of R_L.
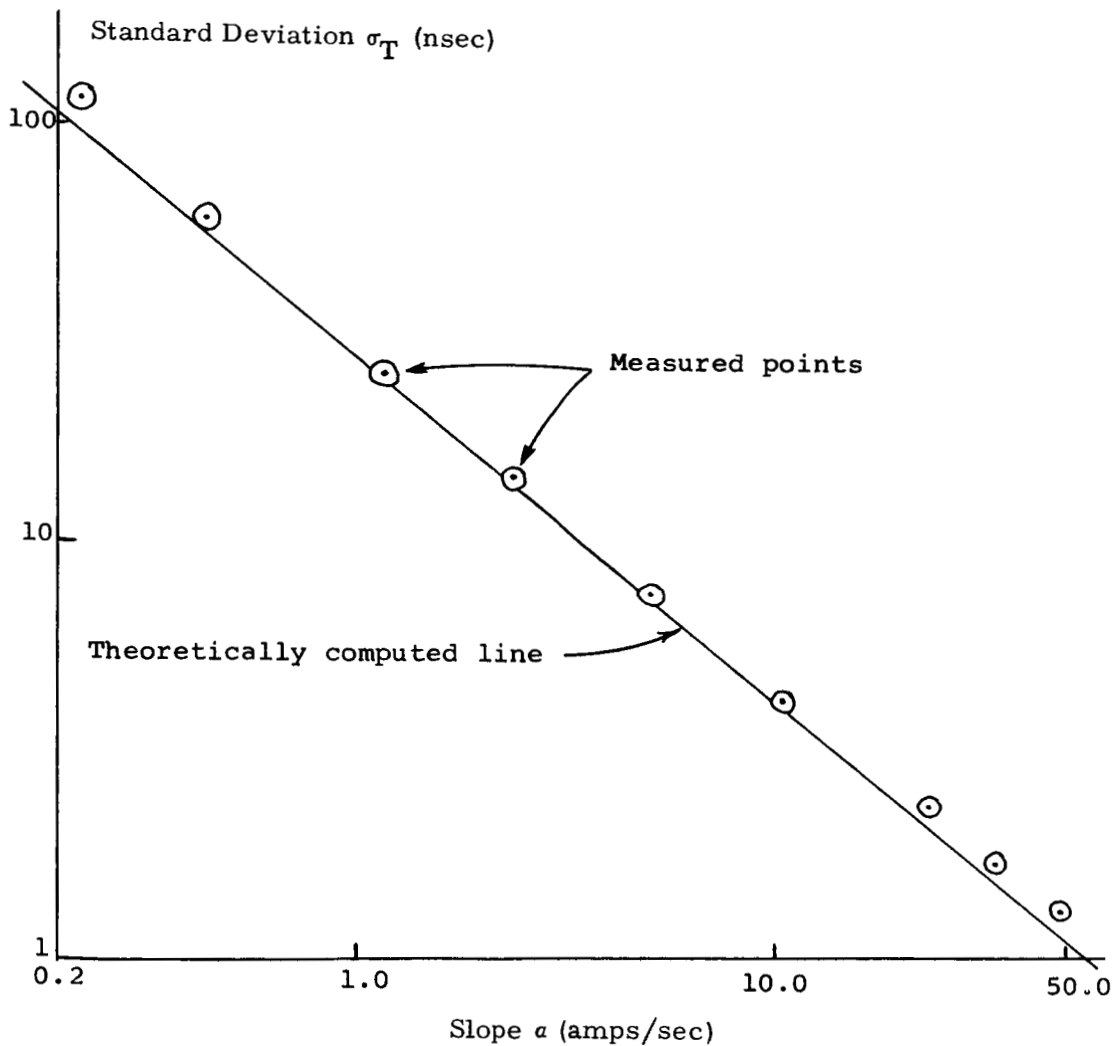
Fig. 12.   Standard deviation σ_T as a function of slope a.

The behavior described by (6) was exhibited over the entire 3.5-decade range of α variation. We expected the jitter to decrease monotonically with slope α but were surprised to find the behavior so regular over so large a range.

c. Dependence of Jitter upon Load Resistance, R_L

If the tunnel diode drive circuit is expressed as an equivalent current-source ramp in parallel with the load R_L, the relation between σ_T and α is, to first order, independent of R_L for R_L greater than 1 kΩ. This result was surprising, as we expected the jitter to be influenced strongly by the load R_L. Plots of σ_T against α for R_L = 1, 2, 4, and 1u kΩ are shown in Fig. 13.
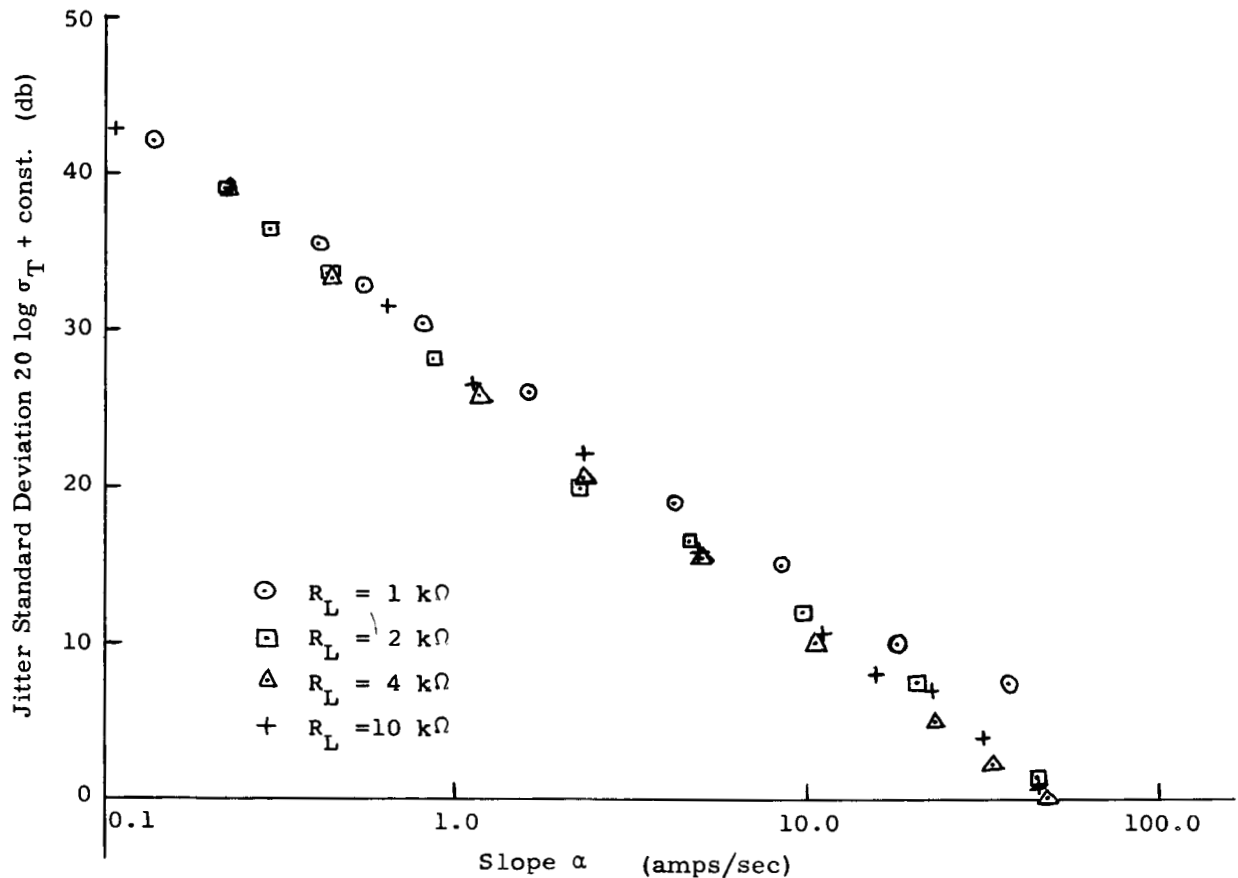
Fig. 13. Jitter standard deviation σ_T versus slope α for several values of R_L.

Of all of the experimental results, this was the most helpful in the obtention of the model presented in Section IV. It focused our attention onto models that did not involve R_L.

IV. MODEL DESCRIBING SWITCHING STATISTICS

We shall now present a model that relates the switching-time randomness to shot noise generated in the tunnel diode and to other circuit parameters. This model will be derived for forward-direction switching, that is, in which the operating point jumps from the peak of the i-v relation, across the valley, to the other stable state.

Three approaches to the problem of modeling jitter in a tunnel-diode switch were considered.

1. An abstract mathematical approach. Procedures that we have found in published works for modeling switching-time randomness were theoretical and quite detached from particular characteristics of any specific physical switching systems. Perhaps, a general model for the class of all physical switching systems does exist, in which case an abstract approach might be fruitful. We were not able, however, to find any general theoretical approach that was simple enough to be applied to our specific tunnel-diode switching problem.

2. A physical approach by using the equivalent linear-circuit model of the tunnel diode. Any approach should, in principle, be relatable to the basic physics of the device, or perhaps to an equivalent-circuit model derivable from the basic physics. A modeling procedure in terms of the equivalent-circuit model described in Section II for the tunnel diode was successful and is the procedure described in this section.

3. An approach based on the microscopic physics of the device. At the outset of the investigation it was not clear that the linear-circuit model could be applied to the modeling of our nonlinear switching process. If this method were fundamentally impossible, then the modeling would most probably have to be done in terms of the microscopic physics of the device. Fortunately, this approach did not have to be used, since the circuit-model approach was successful.

4.1 EQUIVALENT-CIRCUIT MODEL FOR DESCRIBING JITTER STATISTICS

The circuit model used for describing the switching randomness is shown in Fig. 14. The left section is the ramp-generating part of the circuit; the portion on the right is the tunnel-diode model described in Section II.

The ramp generator is expressed in terms of a current rather than voltage-source circuit because the observed statistics were essentially independent of the load R_L for the current drive. The noise source, $n_{th}(t)$, accounts for the thermal noise originating in the load, R_L. The two-sided power-density spectrum of $n_{th}(t)$ has the amplitude

$$N_{th} = \frac{2KT}{R_L}.\tag{7}$$

In the tunnel-diode section of the model, the tunnel diode i-v relation i(v) (shown in Fig. 2), is considered to be instantaneous, or memoryless. The incremental junction

thermal noise
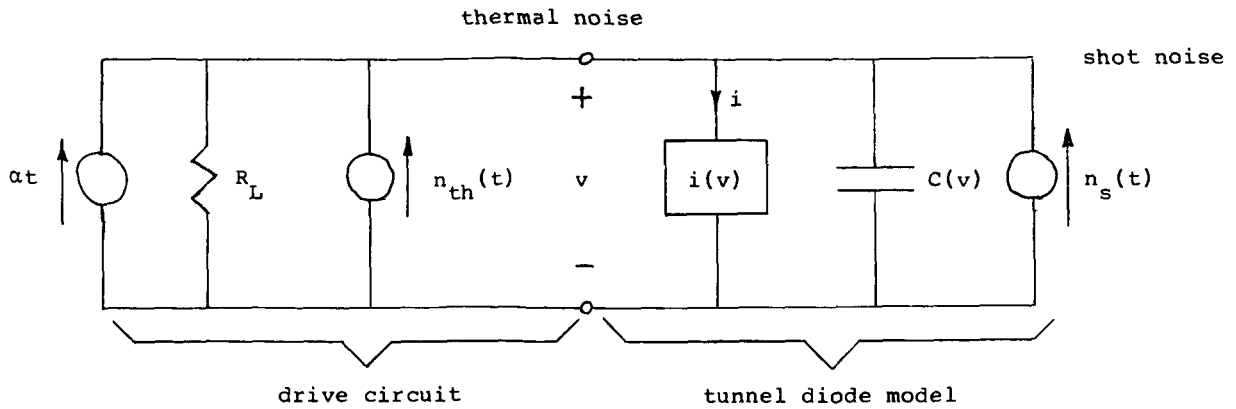
shot noise

Fig. 14. Equivalent-circuit model for tunnel diode threshold-crossing detector.

capacitance, $C(v)$, depends upon voltage. The noise source, $n_s(t)$, accounts for shot noise generated at the diode's junction and has the two-sided spectral height,

$$N_s = qI_{eq}(v), \tag{8}$$

where q is the magnitude of the electron charge, and $I_{eq}(v)$ is the magnitude of the equivalent shot current. The characteristics of the equivalent shot-noise current, $I_{eq}(v)$, were discussed in some detail in Section II. In the region near and to the right of the peak of the diode's i-v characteristic, $I_{eq}(v)$ is approximately equal to the actual diode current, $i(v)$.

a. Some Simplifying Approximations

By observing that the effect of the noise on the switching time is likely to be important in a relatively small operation region, some approximations can be made that greatly simplify the model.

The "decision" to switch is made in the circuit when the operating point is near the

white noise of spectral height N_o

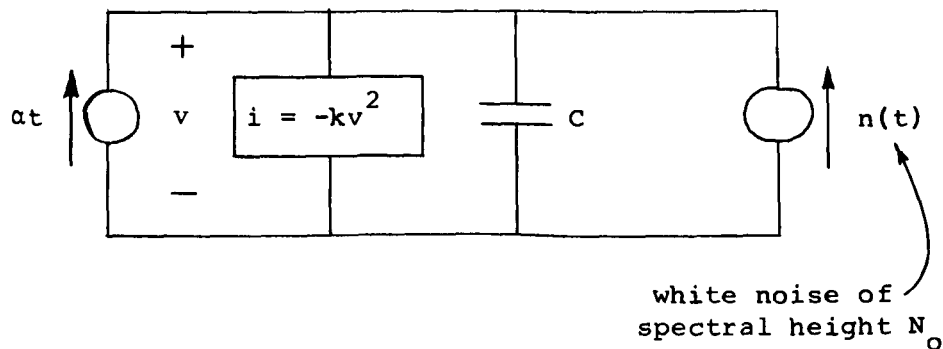Fig. 15. Simplified equivalent-circuit model for the tunnel diode threshold-crossing detector.

20

peak of the i-v curve. If the operating point has not yet reached this critical region, noise perturbations will have a negligible influence on the time of switching. On the other hand, if the operating point is already past this area, the diode is already well on its way toward switching, and further influence from the noise will be insignificant. Thus, switching-time randomness is introduced in a relatively small operating region near the peak of the diode.

A greatly simplified version of the model, shown in Fig. 15, can be obtained by making the following approximations that are accurate over the small critical coupling area.

1. $I_{eq}(v)$ and $C(v)$, moderately dependent on voltage, can be considered to be constant in the critical coupling region near the peak. Thus, in this region, $I_{eq}(v)$ and $C(v)$ can be approximated by

$$I_{eq}(v) = I_{eq}(v_p) = i_p$$

and   (9)

$$C(v) = C(v_p),$$

where v_p is the diode's peak voltage, and i_p, the peak current.

2. The characteristic i(v) can be approximated analytically in the critical peak region. If we expand i(v) about the peak at (v_p, i_p), keeping only terms up to second order, we obtain the new i-v relation,

$$(i-i_p) = -k(v-v_p)^2,$$ (10)

where k is proportional to the curvature at the peak. With no loss in generality, we can translate the i-v coordinate system so that its origin is at (v_p, i_p). Then (10) can be expressed in the simpler form,

$$i(v) = -kv^2,$$ (11)

where it is understood that i and v are new translated variables that are different from those previously used. These variables will be used for the rest of this discussion.

3. Since R_L is a memoryless element, it can be eliminated by combining it with the relation, i(v), which is also memoryless. It is interesting to observe that this does not alter the form of Eq. 11, since the new i-v relation obtained by this combination,

$$i*(v) = -kv^2 + \frac{1}{R_L} v,$$ (12)

is still a parabola with the same second derivative and, consequently, the same value of k.

The white thermal noise, $n_{th}(t)$, originating in R_L, can then be combined with the white shot noise from the diode. The resulting equivalent white noise has

21

the spectral height,

$$N_o = \frac{2kT}{R_L} + qI_{eq}.$$ (13)

At room temperature, for values of R_L that were used ($R_L > 1k\Omega$), and for $I_{eq} = 1$ ma,

$$qI_{eq} \gg \frac{2kT}{R_L}.$$ (14)

Consequently, the shot noise predominates and

$$N_o = qI_{eq}.$$ (15)

4.2 SWITCHING EQUATION

By means of the approximations made in Section 4.1, the much simpler form of the switching model shown in Fig. 15 is obtained. Parameters that depended upon the operating region were considered to be constant over the relatively small region in which the effect of noise upon switching randomness is important. The nonlinear relation i(v) was approximated by a simpler analytic relation.

By using Kirchhoff's current law, the equilibrium equation for the circuit model of Fig. 15 can be written

$$C \frac{dv}{dt} - kv^2 = \alpha t + n(t),$$ (16)

where n(t) is white noise of spectral height N_o, α is the slope of the input current ramp, k is one-half the curvature at the diode's peak, and C is the junction capacitance at the diode's peak. The voltage appearing across the diode is v.

This switching equation, describing the coupling between the noise and the switching time, will be used for deriving the statistics of switching-time jitter.

a. Dimensionless Form of the Switching Equation

By suitably grouping the parameters α, C, and k, we obtain the new dimensionless variables (denoted by primes)

$$v' = \left(\frac{k^2}{C\alpha}\right)^{1/3} v$$

$$\begin{bmatrix} t' \\ \sigma'_T \end{bmatrix} = \left(\frac{k\alpha}{C^2}\right)^{1/3} \begin{bmatrix} t \\ \sigma_T \end{bmatrix}$$

$$N'_o = \left(\frac{k}{C^2\alpha}\right) N_o.$$ (17)

Substitution of these variables in the switching equation (16) results in the alternative dimensionless form of the switching equation,

$$\frac{dv'}{dt'} - v'^2 = t' + n'(t'),$$ (18)

where $n'(t)$ is white noise with spectral height N'_o. The form of any solutions of this equation will depend only on the parameter N'_o.

4.3 SOLUTION OF THE SWITCHING EQUATION

If the noise term were left out of the switching equation (18), the resulting equation would be a form of the Ricatti equation, which appears in numerous physical problems.[6] The solution of this particular form of the equation is a complicated combination of transcendental functions which could not be expressed simply enough to provide insight into our particular problem.

As a result, we have resorted to other methods of interpreting the equation. The first method utilizes dimensional methods and produces, very simply and elegantly, a relation between the standard deviation of the switching-time distribution and the other parameters of the circuit. A linearity assumption is made in this approach that is verified by using a second, more complex, approach: namely, by solving the equation stochastically on a computer. This computer solution also provides us with the complete distribution function of the jitter, together with its relation to the pertinent circuit parameters. These approaches will be described below.

a. Solution by a Dimensional Method

Using dimensional methods only and making one fairly reasonable assumption, we can obtain an expression for the standard deviation σ_T of the jitter.

The assumption is the following: If the noise $n'(t')$ is small enough, then the jitter varies "linearly" with the noise. That is, if we multiply $n'(t')$ by λ then the jitter standard deviation, σ'_T, is also multiplied by λ. Equivalently, if the dimensionless spectral height, N'_o, is small enough, we can write

$$\sigma'_T = A \sqrt{N'_o},$$ (19)

where A is a positive, dimensionless constant.

Simply by transforming the dimensionless σ'_T and N'_o in (19) back into the "dimensional" domain, using (17), we obtain an expression relating σ_T to N_o, a, C, and k. Namely,

$$\sigma_T = \frac{A N_o^{1/2} k^{1/6}}{a^{5/6} C^{1/3}}.$$ (20)

Both the a and C dependence predicted in this relation agree remarkably well with actual observations. A comparison between the theoretical prediction (20) and experimental observations will be given below and in the final summary in Section VI.

b. Complete Solution of the Switching Equation by Computer

A more complete solution of the switching equation is desirable, since the dimensional method gives no information about the switching mean, or about the shape of the jitter distribtion. Furthermore, the validity of the linearity assumption should be checked, and the proportionality constant, A, evaluated.

The switching action was simulated on an IBM 7094 computer by digitally solving the dimensionless switching equation (18). Standard difference techniques were used. Noise was obtained by means of a standard random-number-generating routine, and was introduced at each iteration of the difference equation. The random-number sequence was zero mean and had a variance that was adjusted to correspond to a desired value of N_o'. The random numbers were rectangularly distributed.

For a selected value of N_o', by using initial conditions corresponding to equilibrium at $T' = -\infty$, the equation was solved 1000 times, the solution yielding that many values of the random switching time, T_s'. Then the standard deviation, σ_T, the switching-time mean, $\overline{T_s}$, and the distribution of T_s were computed by using standard techniques. This procedure was repeated for each of several values of N_o'. A more detailed discussion of the computing techniques that were used is presented in Appendix C.

c. Computed Jitter Statistics

The Distribution

For each value of N_o', 1000 values of the random switching time T_s' were obtained. Then from these points, the distribution was computed. A typical distribution is shown in Fig. 16. A plot of this distribution on probability paper is presented in Fig. 17. The fluctuations in the distribution are statistical fluctuations that arise because only 1000 data points were used.

The distributions begin to deviate from Gaussian for $N_o' > 2$. This is probably due to the fact that we were not able to start the waveform back far enough in time for the larger values of N_o'. The larger the value of N_o', the farther back in time the initial starting time would have to be in order to ensure a condition equivalent to commencement in equilibrium at $t' = -\infty$. If the starting time were pushed back too far, the time required for computation would become objectionably long.

Thus we have been able to solve the model for its predicted distribution only for $N_o' \leq 2$. No conclusions can be made at this time concerning the distribution for $N_o' > 2$.

It is interesting that the computed switching time distribution was Gaussian-shaped, even though the input noise was rectangularly distributed. This can be explained heuristically in terms of the model.

When $v'(t')$ is small just before switching, the circuit acts approximately as

Number of points per channel

channel width = .05 dimensionless "seconds"
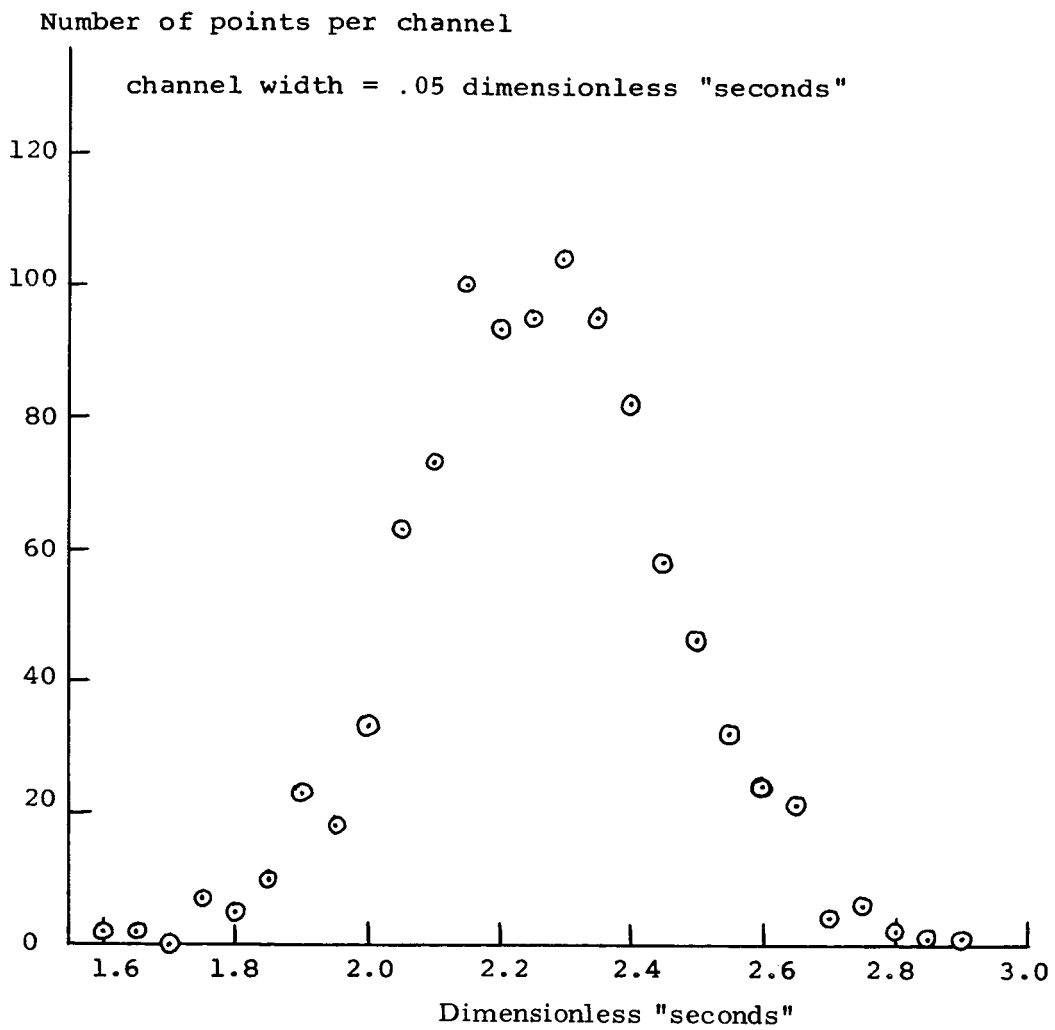

Dimensionless "seconds"

Fig. 16. Typical computed distribution $P_{T'_s}(t')$. $N'_o = 0.1$. Number of samples: 1000.
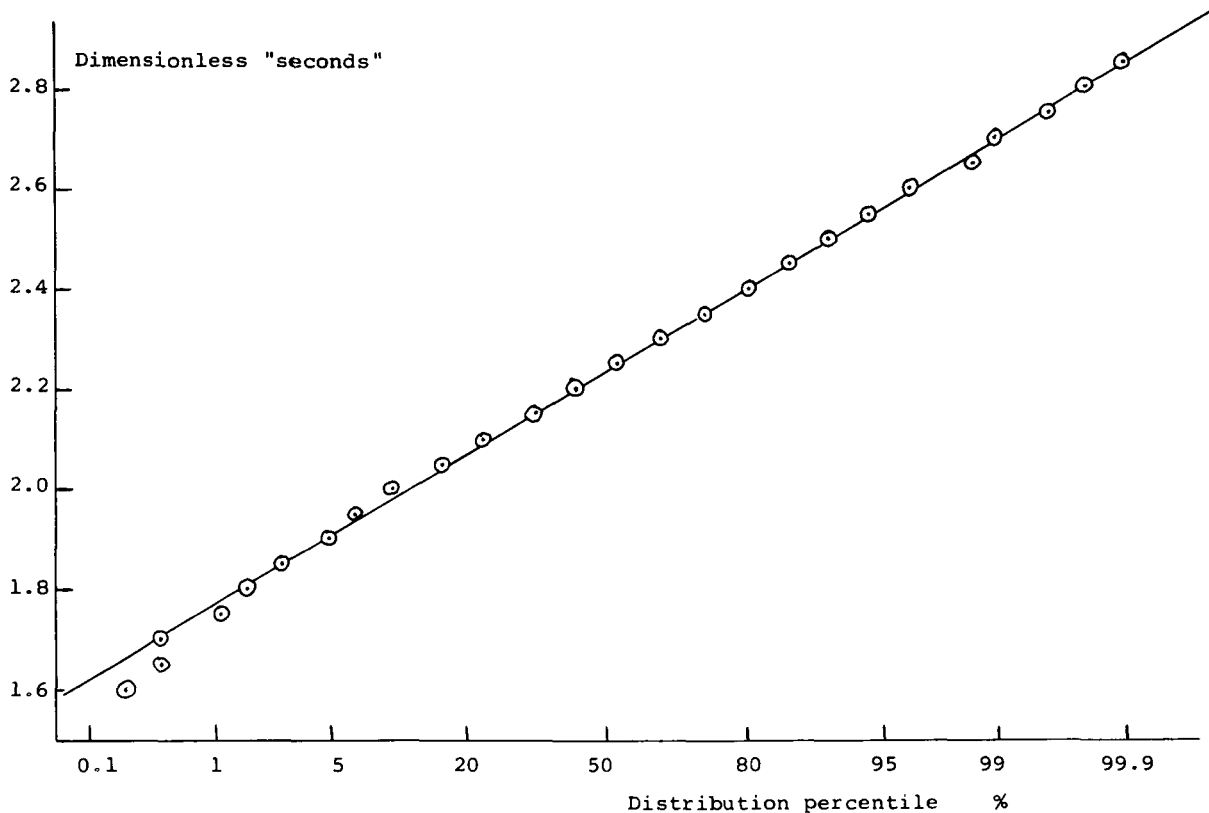
Fig. 17. Plot of theoretically computed integrated distribution of T'_s on probability paper. $N'_o = 0.1$. Number of samples: 1000.

a capacitor, or as a pure integrator. If non-Gaussian white noise is applied to a very narrow-band system such as our "integrator," the output process will be close to Gaussian. Since the relation between noise and jitter is "linear" (a result that is presented in the next section) and T'_s is obtained by integrating over the noise, it is not unreasonable that T'_s be Gaussian.

Jitter Standard Deviation and Mean as a Function of Spectral Height N'_o

A Gaussian distribution is completely specified if its mean and standard deviation are determined. Consequently, if we know $\overline{T'_s}$ and σ'_T as a function of noise spectral height N'_o, we shall have completely determined the statistics of the switching time. By transformation back into the dimensional domain, the statistics will then be specified in terms of all of the pertinent dimensional parameters: slope a, curvature $-2k$, junction capacitance C, and noise spectral height N_o.

The computed relations between σ'_T and N'_o, and $\overline{T'_s}$ and N'_o are shown in Figs. 18 and 19, respectively. These relations can be approximated analytically by the expressions
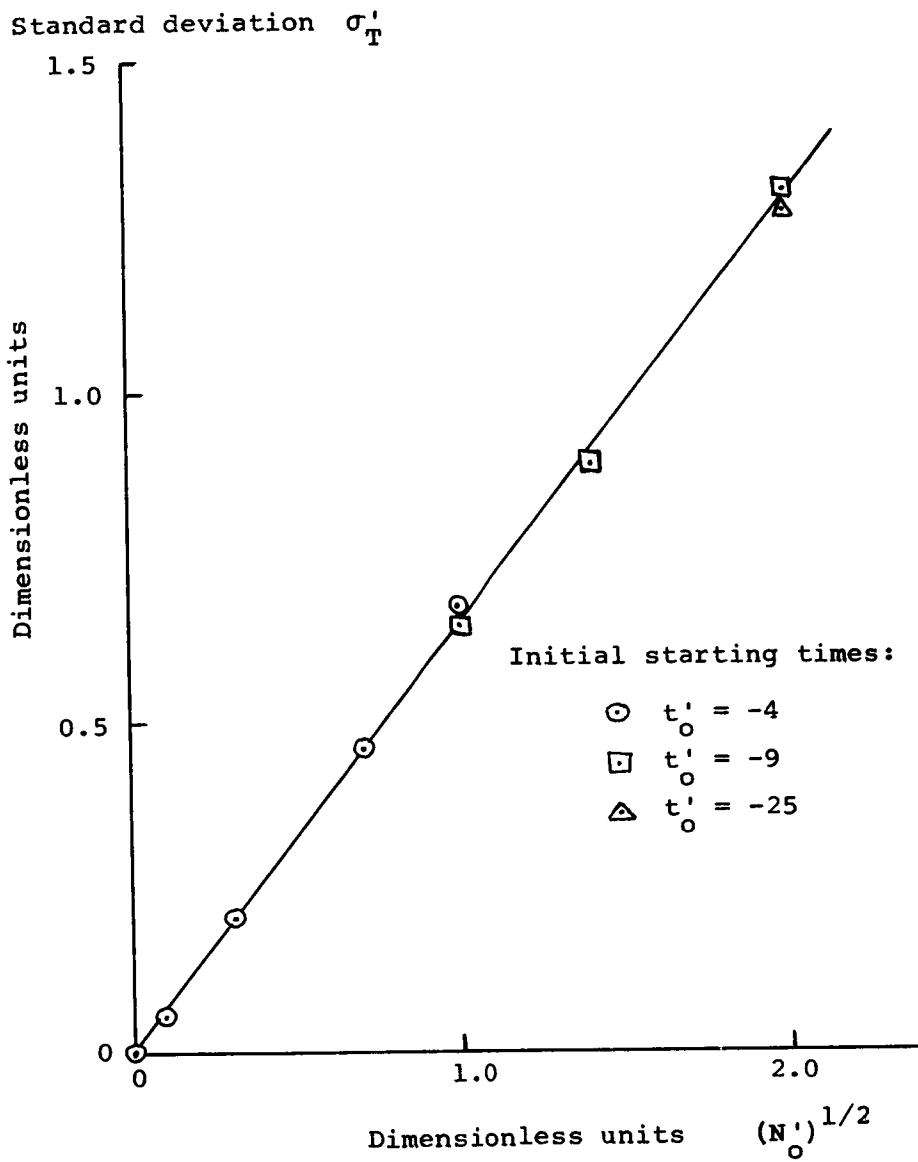
Fig. 18. Switching-time standard deviation, σ_T', vs noise spectral height, N_o'.

$$\sigma'_T(N'_O) = A \sqrt{N'_O}$$

and

$$\overline{T'_S(N'_O)} = \beta - \gamma N'_O, \tag{21}$$

where $A = 0.65$, $\beta = 2.33$, and $\gamma = 0.30$.

That $\sigma'_T(N'_O)$ varies linearly with N'_O supports the linearity assumption that was made for the solution by the dimensional method.
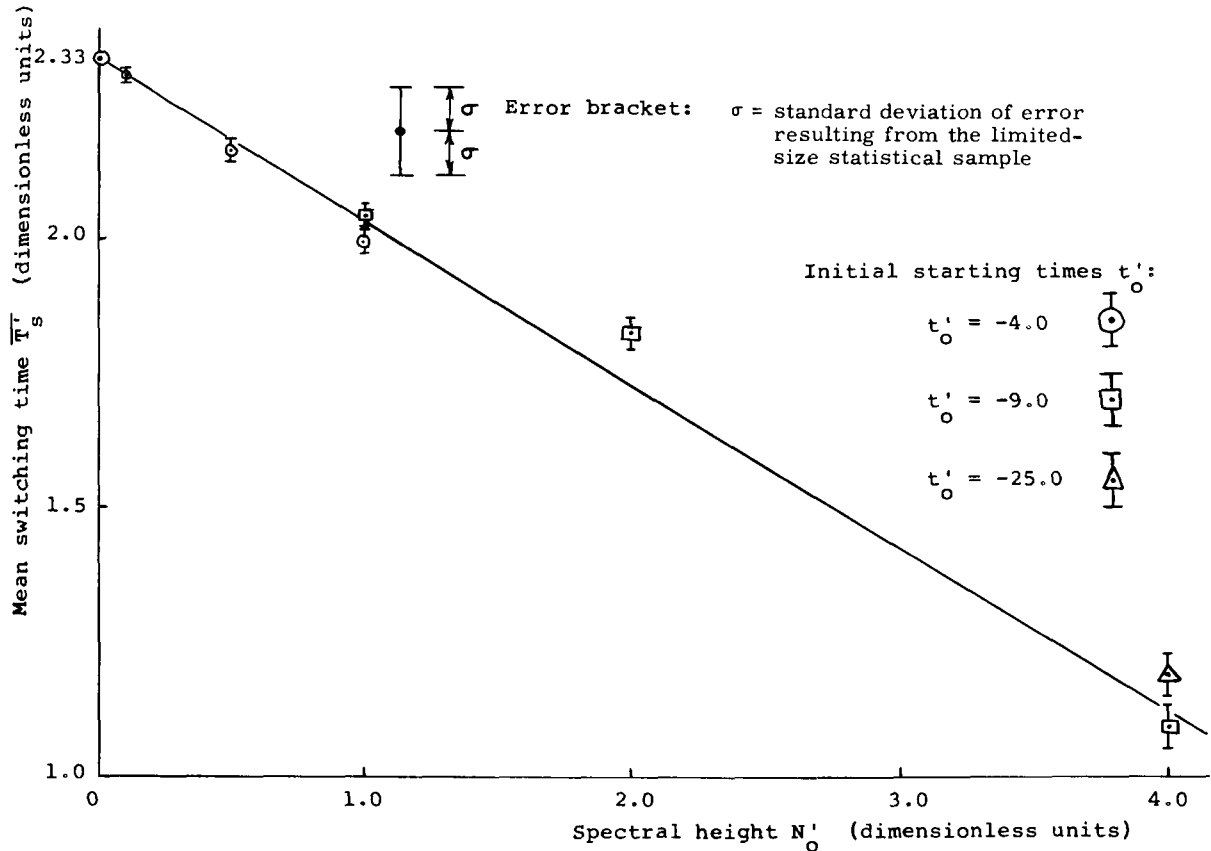
Fig. 19. Mean switching time, $\overline{T'_S}$, vs noise spectral height, N'_O.

The wide deviations of several of the points on the graph are due to two factors: (i) statistical fluctuations resulting from the limited 1000-point sample size, and (ii) deviations attributable to an initial starting time that was not back far enough. The standard deviation of the statistical error in the point locations is indicated by the error brackets shown in Fig. 19.

It is interesting that the standard deviation, σ'_T, hardly depends on the initial starting time at all, whereas the switching mean, $\overline{T'_S}$, is highly sensitive to the starting time.

We felt that it would not be worth while to repeat the computation for starting times

28

that were back far enough, since several hours of additional computer time would have been required. As a result, the theoretical computation of $\overline{T_s'}$ is not as accurate as might be desired. The computation does indicate the general linear behavior of $\overline{T_s'(N_o')}$, but does not show how the linearity breaks down, if it does.

For all experimental measurements that were made, $N_o' < 1.5$. This value was computed with the use of Eq. 17 and the parameter values $k = 1/7$ amp/volt^2, $I_{eq} = 1$ ma, and $C = 10$ pf. The minimum slope, corresponding to the maximum value of N_o', was $\alpha = 0.2$ amp/sec.

$\sigma_T'(N_o')$ was linear for all values of N_o' that were used (up to $N_o' = 4$). This certainly includes the range of $N_o'(N_o' < 1.5)$ covered in the experimental measurements. Although we did not measure the switching mean experimentally, we see that the theoretical behavior of $\overline{T'(N_o')}$ is also approximately linear over the measurement range, $N_o' < 1.5$.
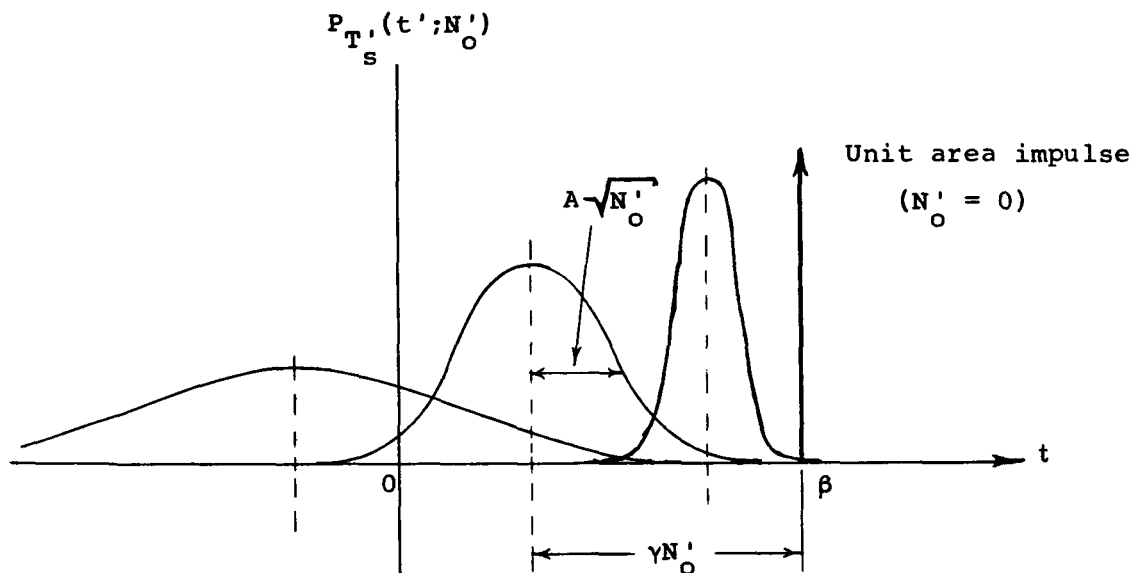
Fig. 20. Gaussian-shaped switching distribution moves to left and widens as noise spectral height is increased.

The behavior of the distribution, $P_{T_s'}(t';N_o')$, of T_s' with N_o' as a parameter is shown in Fig. 20. With no noise, switching occurs with probability one at the delayed time β. As N_o' is increased, switching occurs earlier, on the average. This is because the noise peaks are more likely to cause switching to occur earlier than later.

An interesting observation can be made: $P_{T_s'}(t';N_o')$ satisfies the differential equation for diffusion in a moving medium. This observation suggests that another, perhaps more fundamental, approach to the problem might exist. Thus far we

have not been able to derive the differential equation directly from the switching model.

<center>Dimensional Forms of $\sigma'_T(N'_o)$ and $\overline{T'_s(N'_o)}$</center>

By substituting the transformation relations of (17) in (21), we obtain the expressions relating the dimensional standard deviation, σ_T, and mean, $\overline{T}_s$, to the circuit and device parameters, a, C, and k:

$$\sigma_T = \frac{AN_o^{1/2}k^{1/6}}{a^{5/6}C^{1/3}}$$

$$\overline{T}_s = \left(\frac{C^2}{ka}\right)^{1/3}\left[\beta - \gamma\frac{kN_o}{C^2a}\right]. \tag{22}$$

In these expressions, N_o is the spectral height of the noise (shot noise in the device); C, the capacitance across the tunnel-diode junction; k, one-half the curvature at the current peak; a, the slope of the input current ramp; and A = 0.65, β = 2.33, and γ = 0.35.

The switching-time distribution, $P_{T_s}(t)$, is obtained simply by substituting the relations (22) for σ_T and $\overline{T}_s$ in the Gaussian form:

$$P_{T_s}(t) = \frac{1}{\sqrt{2\pi}\,\sigma}\exp\left[-\frac{1}{2}\frac{(t-T_s)^2}{\sigma_T^2}\right]. \tag{23}$$

d. Independence of Jitter Standard Deviation σ and Load Resistance R_L

In Section III we stated that the experimentally determined jitter standard deviation, σ_T, is independent of the load R_L when R_L is large enough and the drive is expressed as a current-source ramp in parallel with the load. We shall now show that the model predicts this behavior.

In analyzing the model we simplified the instantaneous relation, i(v), by approximating it with the parabola, $-kv^2$, in the critical switching region near the peak.

We can incorporate R_L into the model by including it in the instantaneous i-v relation, i(v), thereby obtaining the new relation,

$$i(v) = -kv^2 + \frac{1}{R_L}v. \tag{24}$$

Regardless of the value of R_L, the new relation i(v) will still be a parabola with a second derivative, $-2k$, that is independent of R_L. Since the standard deviation σ_T depends only on k, and since the new parabola has the same value of k as the old,

<center>30</center>

regardless of the value of R_L, σ_T will be independent of R_L.

The "critical region," where the effect of noise on the jitter is most important, is that area near the point of tangency of the load line with the current peak. If R_L is made too small, the critical region will move to the right, away from the peak of the i-v relation where the original parabolic assumption was valid. If R_L is made much smaller, switching will not occur, since the load will always intersect i(v) in only one point. Consequently, if R_L is much larger than the magnitude of the minimum negative resistance of the diode, the critical switching region will be near the peak, and the jitter standard deviation σ_T will be independent of R_L.

e. Agreement between the Model's Predictions and Actual Measured Results

At this point, three comparisons can be made between predictions of the model and measured results.

1. Remarkably good agreement has been obtained for the relation between the jitter standard deviation σ_T and the slope a. In Fig. 12 the theoretical relation (24) is superposed on the experimental points.

2. The model predicts the observed result that σ_T is independent of load resistance R_L when R_L is much larger than the minimum negative resistance of the diode.

3. The model predicts that the jitter distribution should be Gaussian. This agrees with the observed results.

The theoretical results presented here motivated some additional experiments that could be performed to further check the validity of the model. Discussions of these other experiments are presented in Section V.

31

V. EXPERIMENTS CONCERNING OTHER PREDICTIONS AND EXTENSIONS
OF THE MODEL

The experiments presented in Section III were motivated during the process of formulating the model. They furnished insight that was useful in obtaining the model. Certain other experiments were performed to test predictions and extensions of the model.

It is generally desirable that the validity of the various predictions and extensions of the model be checked as much as is feasible. If any prediction does not agree with experimental facts, then the model is deficient, and should be modified or rejected, or the limits of its validity should be established. On the other hand, if agreement is obtained, the model is strengthened and rendered more useful, since its known range of applicability is increased.

We shall now describe three experiments: (i) Variation of the jitter standard deviation as a function of diode size; (ii) Variation of jitter standard deviation as a function of capacitance added externally across the diode; and (iii) Jitter statistics for switching in the "reverse direction" — from the valley of the i-v curve back to the original state.

The first and second experiments concern relationships that are predicted by the model that was derived in Section IV for forward-direction switching. The third investigation was performed to determine whether that model would also hold for reverse switching.

We found experimentally that the forward-switching model did not describe the jitter occurring in the reverse-direction case. Consequently, another model was developed for this situation. This model, presented in section 5.3, exhibits all of the characteristics that were experimentally observed.

5.1 VARIATION OF JITTER STANDARD DEVIATION WITH DIODE SIZE

If we assume that a larger diode can be expressed equivalently as several smaller ones in parallel (for example, a 2-ma diode would be equivalent to two 1-ma diodes in parallel), then we can easily derive the theoretical dependence of the jitter standard deviation, σ_T, upon the diode size.

With this assumed scaling, if a diode's size is scaled by the factor x, then its capacitance C, shot-noise spectral height N_o, and curvature, $-2k$, will also be scaled by x.

It should be pointed out that this assumed scaling law is only approximate. For small diodes, leakage and field fringing cause this scaling relation to break down. According to the manufacturer's specifications for the diodes that were used, the assumed scaling is accurate within approximately 10%.

Let the jitter standard deviation corresponding to the original diode be denoted σ_o, and that for the scaled diode σ_x. Then by using the previously derived relation

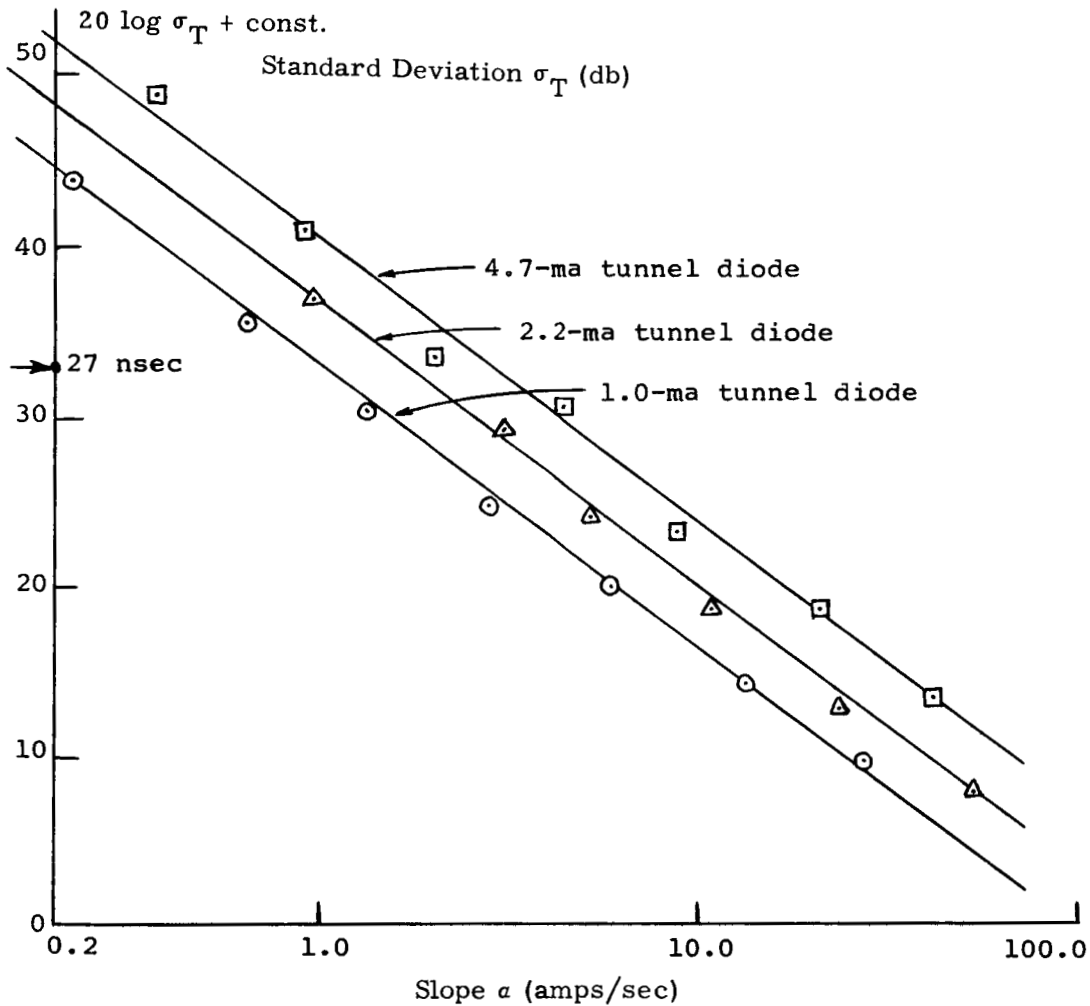$$\sigma_T = \frac{AN_o^{1/2}k^{1/6}}{a^{5/6}C^{1/3}},$$

(25)

Fig. 21. Jitter standard deviation as a function of input slope for 1.0, 2.2, and 4.7-ma germanium tunnel diodes. Straight lines with the theoretical −16.6 db/decade slope were visually fitted to the measured points.

the ratio σ_x/σ_o for fixed a can be expressed as

$$\frac{\sigma_x}{\sigma_o} = x^{1/3}. \tag{26}$$

The jitter standard deviation σ_T was measured as a function of slope a for 1, 2.2, and 4.7-ma germanium tunnel diodes (G.E. Types 1N3713, 1N3715, and 1N3717, respectively). These measured results, shown in Fig. 21, support the theoretical scaling of Eq. 26.

a. Optimally Sized Diode for Least Jitter

The theoretical relation (26) implies that the jitter can be made arbitrarily small by using a small enough diode. In actual practice, however, the relative amount of surface

leakage increases as the diode size is decreased. This causes the relative depth of the valley to decrease, which, in turn, results in slower switching speeds. Finally, if the diode is made too small, the shunt leakage becomes large enough to cancel out the negative resistance, thereby making the i-v relation single-valued in current — and making switching impossible.

5.2 VARIATION OF JITTER STANDARD DEVIATION WITH JUNCTION CAPACITANCE

The model predicts (see Eq. 25) that the variation of the standard deviation σ_T with the net junction capacitance should be
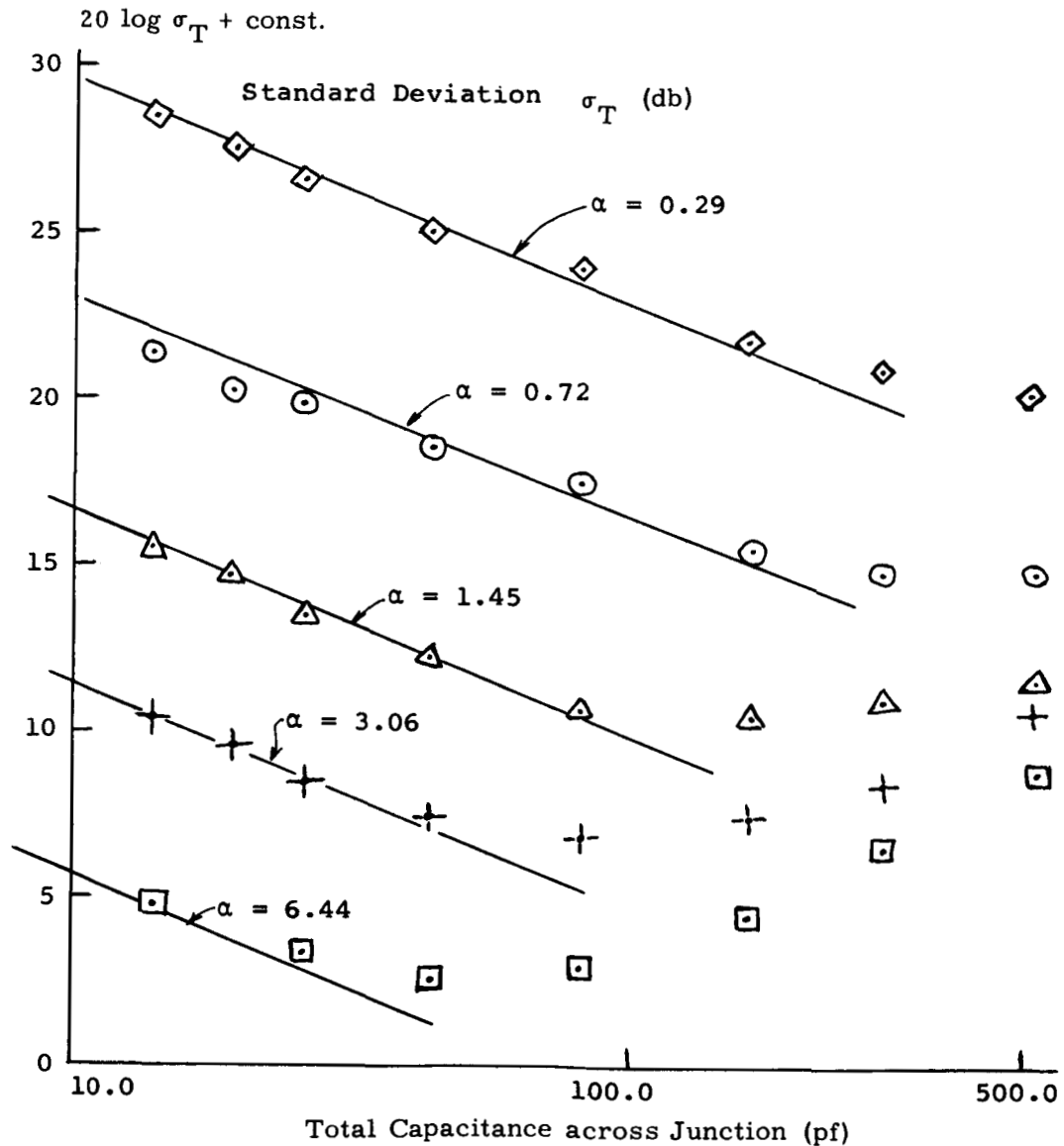

Fig. 22. Jitter standard deviation σ_T vs total capacitance C across junction for several values of slope a. The lines shown have a theoretical slope, −6.6 db/decade, and were visually fitted to the points.

34

$$\sigma_T \sim \frac{1}{C^{1/3}}. \tag{27}$$

To check this result experimentally, σ_T was measured as external capacitance was added across the junction. The net capacitance C across the junction would then be

$$C = C_{ext} + C_{int}, \tag{28}$$

where C_{ext} is the externally added capacitance, and C_{int}, the diode's intrinsic capacitance.

The experimentally determined relation between σ_T and C for several values of the slope a is plotted in Fig. 22. This measured behavior agrees with the theoretically predicted relation (27), as long as the capacitance is not made too large. When C is made too large the jitter actually increases with C, contrary to the prediction of the model.

This discrepancy may be due to series inductances in the diode and capacitor leads which were not included in the model. With the inductance included, the junction would see the L-C circuit shown in Fig. 23. The discrepancy may result because this circuit is inductive above the series-resonant frequency,

$$f_o = \frac{1}{2\pi \sqrt{LC_{ext}}} \tag{29}$$

where L is the lead inductance. In the model it is assumed that the diode sees a pure capacitance.
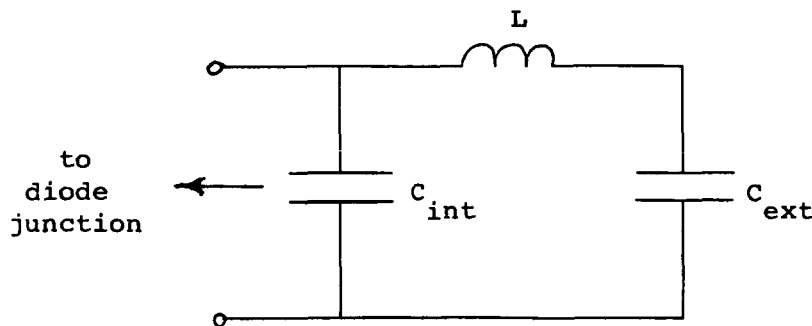
Fig. 23. Equivalent L-C circuit that appears across the diode junction when external capacitance, C_{ext}, is connected across the diode. Series lead inductance is shown.

For our measuring conditions, $L \cong 10^{-8}$ hy and $C_{ext} \cong 200$ pf, resulting in $f_o \cong$ 100 Mc. The shot noise generated in the diode is white well beyond 100 Mc. Furthermore, since the switching rise time is approximately 10 nsec, much of the energy generated during the switching transient falls into frequencies of the order of 100 Mc.

Consequently, the inductive effect may well be the cause of the discrepancy.

No attempt was made to provide low-inductance mounts for the diodes during the experiment.

5.3 REVERSE-DIRECTION SWITCHING

Measurements of the jitter statistics were made for switching in the reverse direction, that is, from the valley back to the original state, as shown in Fig. 2, to check the applicability of the jitter model in this case.

We expected a priori that there would be much less jitter for reverse than for forward switching because the equivalent shot noise in the valley is much less than that near the peak. (At that time we had not taken the $1/f$ noise into account.) We were surprised, however, to find that there was slightly more jitter for the reverse case.

Upon closer examination we found that the variation of the standard deviation, σ_T, with slope a is

$$\sigma_T \sim \frac{1}{a}. \tag{30}$$

Also, σ_T was found to be independent of capacitance added externally across the junction (700 pf was the largest value used).

These observations do not agree with the corresponding relation predicted by the forward-switching model,

$$\sigma_T \sim \frac{1}{a^{5/6} C^{1/3}}. \tag{31}$$

Thus we conclude that the model derived for forward switching is not suitable in the reverse-switching case.

a. Model for Reverse-Direction Switching

We shall present a model that explains qualitatively the behavior observed above for reverse-direction switching. We shall show, first, that the jitter is most probably related to $1/f$ noise (white shot noise was the source of jitter in the forward-direction case). Then, by making some reasonable assumptions concerning the characteristics of the $1/f$ noise, a model is obtained that exhibits the experimentally observed behavior.

Source of Jitter for Reverse Switching

A possible cause for the observed difference between forward and reverse switching can be seen by examining the tunnel diode model presented in Section II.

For reverse-direction switching the "critical region" for coupling between noise and jitter is the valley region (near the point of tangency between the load line and the i-v characteristic). Since low-frequency $1/f$ noise is prevalent in this region, it is most apt to be the source of the jitter.

The Model

The model will be derived by using the equivalent-circuit model for switching presented in Sections II and IV. The circuit model for reverse switching, shown in Fig. 24, -
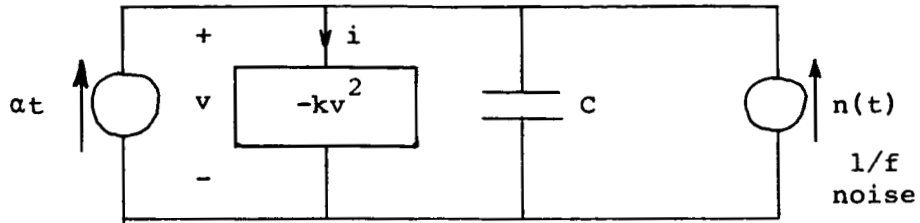
Fig. 24. Equivalent-circuit model for describing jitter statistics in reverse-switching case.

differs from that previously used for forward switching, in that k and C now have the values that exist in the "critical coupling region" in the valley of the diode's i-v characteristic. The noise n(t) is $1/f$ noise.

For reverse switching, a and k would normally be negative. To avoid this change in signs, we let a and k be the magnitude of the respective parameters.

Fig. 25. Illustrating the geometric relationship between the noise and switching-time distributions.

The noise n(t) has the property that its power is concentrated in very low frequencies and that it exhibits approximately a $1/f$ spectrum. Now let us assume that n(t) varies slowly enough so that the following conditions are satisfied:

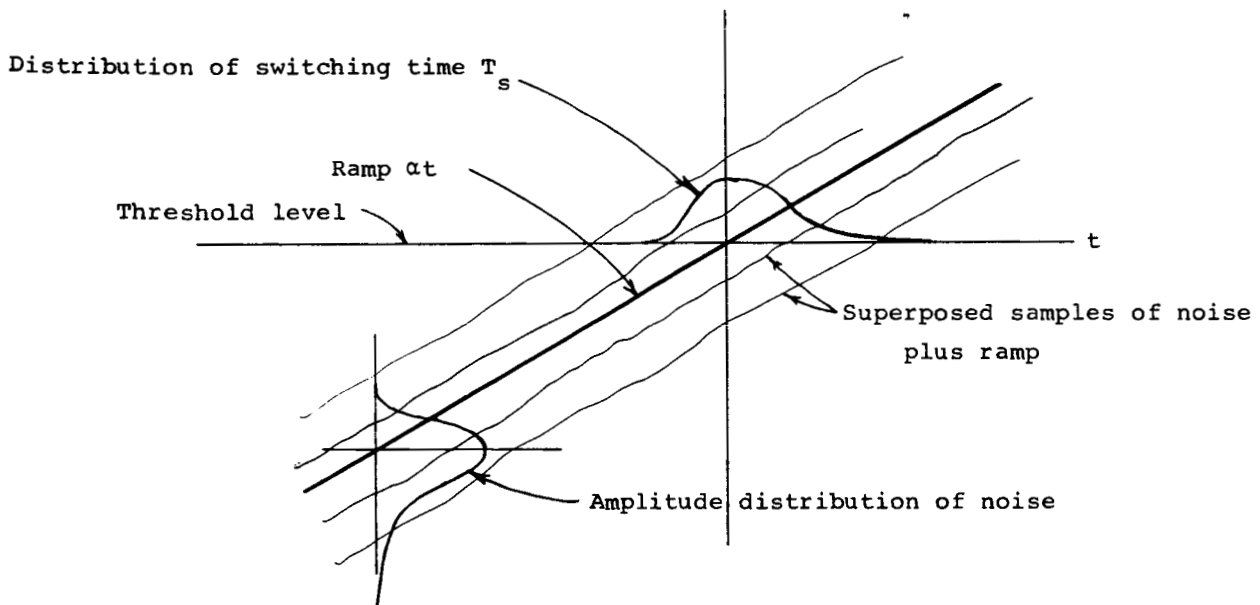1. The time interval over which the "decision" to switch is made is much smaller than intervals over which appreciable variations in n(t) occur. That is, the amplitude of the noise is practically constant while the operating point is in the critical coupling region.

2. For large enough values of slope a, the slope of $at + n(t)$ is very close to a, most of the time. This means that the effect of the noise would be simply to displace the ramp vertically, without changing its slope. Typical sample functions of ramp plus noise satisfying this condition are shown in Fig. 25.

Now consider some of the consequences of these assumptions. The first assumption implies that, except for a deterministic time delay, the diode can be considered to switch at the instant the ramp plus noise first crosses the threshold level (in this case, the level zero).

Thus the equivalent switching model can be redrawn as shown in Fig. 26, where the ramp plus noise is applied to a threshold crossing detector that is considered to switch the instant the input first crosses the threshold level (we are neglecting the deterministic time delay). It is interesting to observe that in this situation, the jitter will be independent of the capacitance C (as was experimentally observed), and also of k.

An implication of the second assumption can be seen by examining Fig. 25. Because

$$\frac{d}{dt}\left[at + n(t)\right] = a, \tag{32}$$

the noise projects geometrically onto the time axis. That is, if the noise, n(t), has the value n on a given observation, then the switching time, T_s, for that observation will be given by

$$T_s - \overline{T_s} = \frac{n}{a}, \tag{33}$$

where $\overline{T_s}$ is the mean switching time. By using this transformation relation between the random variables T_s and n, the desired statistics of T_s can be obtained in terms of the

First-passage-time detector
(threshold level at zero)
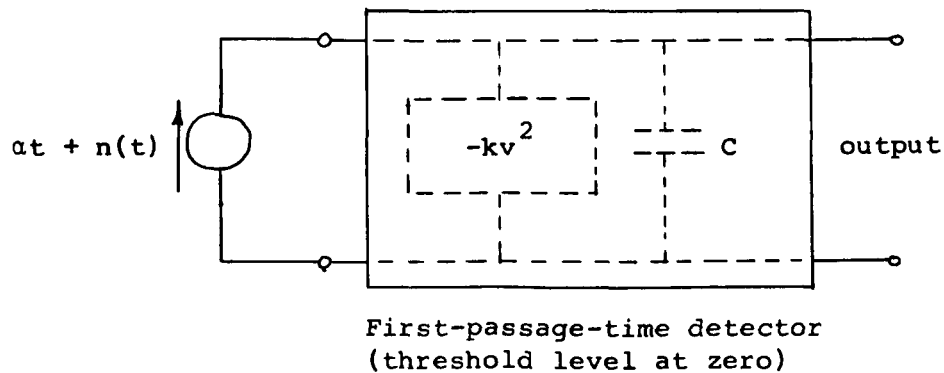
Fig. 26. Reverse-switching problem expressed as a first-passage-time problem.

38

first-order statistics of n(t).

By means of (33), the relation between the switching-time standard deviation, σ_T, and the noise standard deviation, σ_n, can be written

$$\sigma_T = \frac{\sigma_n}{a}. \tag{34}$$

This result agrees with the experimentally observed relation (30) between σ_T and a.

The switching-time distribution, $P_T(T_s)$, can be expressed in terms of the amplitude distribution of the noise, $P_n(x)$, by using the transformation (33). Namely,

$$P_T(T_s) = \frac{1}{a} P_n[a(T_s - \overline{T_s})]. \tag{35}$$

No measurements were made of either $P_T(T_s)$ or $P_n(x)$.

VI. SUMMARY AND CONCLUSIONS

As much emphasis has been placed on the approach and thinking used in obtaining the jitter model as was placed on the actual theoretical and experimental results. As a consequence, descriptions of the specific characteristics of the switching randomness are somewhat scattered throughout this report.

These results will now be consolidated. Predictions of the model and experiments that were performed to check these predictions will be summarized. Following the summary, conclusions and suggestions for approaching the general problem of modeling jitter in other kinds of switching circuits will be presented.

We have observed experimentally that the jitter characteristics for forward switching (from the peak of the i-v curve, across the valley to the other state) were quite different from the corresponding characteristics for switching in the other direction (from the valley of the i-v curve, back to the initial state). Different models were required to describe the jitter in the two cases.

6.1 SUMMARY OF JITTER STATISTICS FOR FORWARD SWITCHING

The model describing the statistics of the switching-time randomness for forward switching was presented and discussed in Section IV. We shall briefly review its development and summarize its predictions.

First, we assumed that noise in the tunnel-diode circuit would have the strongest influence on the switching time when the operating point is in the region where the diode is effectively "deciding" to switch. This "decision" region is the vicinity near the peak of the diode's i-v characteristic.

A small-signal noise model for the diode was approximated analytically in this critical decision region and an equivalent circuit model was obtained.

By using Kirchhoff's current law, the equilibrium equation for the equivalent circuit model was found to be

$$C \frac{dv}{dt} - kv^2 = \alpha t + n(t), \tag{36}$$

where C is the diode's junction capacitance, k is one-half the curvature of the i-v characteristic at its peak, α is the slope of the input signal applied to the switch, n(t) is white noise that is a combination of thermal and shot noise in the circuit, and v is the voltage across the diode.

This equation, which describes the voltage appearing across the diode as switching is commencing, was used to obtain the complete statistical description of the switching-time randomness in terms of the circuit and diode parameters. The interpretation and solution of the equation has been described in Section IV.

40

a. Predictions of the Model

The predictions of the switching model are summarized below.

1. The distribution of the switching times was Gaussian. This distribution was computed theoretically from the switching equation (36). This distribution is Gaussian, even if the white-noise process, n(t), is not Gaussian. The range of parameter values over which the computations were made amply covers the range over which experimental measurements were made.

2. The switching-time mean and standard deviation were also obtained and are given by

$$\sigma_T = \frac{A N_o^{1/2} k^{1/6}}{a^{5/6} C^{1/3}} \tag{37}$$

and

$$\overline{T}_s = \left(\frac{C^2}{ka}\right)^{1/3} \left[\beta - \gamma \frac{k N_o}{C^2 a}\right], \tag{38}$$

where σ_T is the switching-time standard deviation, $\overline{T}_s$ is the mean, N_o is the spectral height of the white noise, k is one-half the curvature at the tunnel diode peak, and a is the slope of the input ramp. In the expression, A = 0.65, β = 2.33, and γ = 0.30. The computations of (37) and (38) were made over a limited range that amply covers the range over which the experimental observations were made.

3. The jitter standard deviation, σ_T, is independent of the load resistance R_L when the drive circuit is expressed as a current-source ramp in parallel with the load R_L, and when R_L is much greater than the minimum magnitude of the negative resistance of the tunnel diode's i-v characteristic. (For a 1-ma germanium tunnel diode at room temperature this minimum negative resistance is approximately $125\,\Omega$.)

b. Experiments Performed to Check the Model

The experiments that were performed to check the validity of the model are summarized below.

1. Switching-time distributions were measured for a wide range of input slopes. In all cases the distributions were Gaussian within the measurement accuracy. The observation supports the corresponding theoretical result.

2. The switching-time standard deviation, σ_T, was measured as a function of input slope a. Measurements were made over approximately a four-decade range of a variation. The measured points support the theoretically predicted relation (37) within the measurement accuracy of approximately 5 per cent. See Figs. 12, 13, and 21 for typical plots of σ_T against a.

3. The standard deviation σ_T was measured as a function of slope, a, for load

resistances of 1, 2, 5, and 10 kΩ. The measured relation between σ_T and a was essentially independent of the load R_L for those values. This observation supports the corresponding predicted result. This experiment has been described in Section III.

4. The relation σ_T versus a was measured for tunnel diodes of different peak currents. By neglecting fringing and shunt leakage across the diode, a reasonably simple scaling law for the diode's parameters was assumed (this law agreed with the manufacturer's specifications within 10 per cent for the diodes used). For this law it was shown that the standard deviation, σ_T, of the jitter should vary as the diode's peak current to the one-third power.

5. The standard deviation, σ_T, was measured as a function of capacitance added externally across the junction. The experimental results followed the predicted relation (37) as long as the capacitance was not too large. (See Fig. 22 for a plot of the measured results.) A hypothesis explaining the discrepancy for the larger capacitance values is presented, together with a description of the experiment, in Section V.

Measurements were made of σ_T versus a for 1, 2.2, and 4.7-ma diodes. The results obtained essentially agree with the predicted result. This experiment has been described in detail in Section V.

6.2 JITTER STATISTICS FOR REVERSE SWITCHING

We have found experimentally that the model that was derived for forward switching did not describe the jitter in the reverse-switching case. Another model was derived that relates the jitter to 1/f noise occurring in the tunnel diode. This model has only been partially verified experimentally, since some of the assumptions made concerning the 1/f noise have not been checked experimentally.

The entire discussion concerning reverse-direction switching has been presented in Section V; therefore, a summary will not be presented here.

A complete description of the statistics of switching jitter has been obtained for the tunnel-diode switch. This description per se is perhaps not the most significant contribution of this report. That we have shown that jitter can indeed be modeled for one of the many switching circuits of interest may be far more significant. We may have pointed a way toward the modeling of jitter in other kinds of switching circuits.

Having demonstrated that the randomness in a tunnel diode switch, which, of course, is highly nonlinear, can be modeled in terms of the small-signal (linear) noise models of the circuit components comprising the switch is in itself a useful contribution. It is this approach that may be useful in obtaining models for other kinds of switches and threshold detecting devices.

6.3 MODELING OF JITTER IN OTHER KINDS OF CIRCUITS

One might wonder whether the jitter models for other types of switching circuits, such as the Schmidt trigger, flip-flop, and neon-bulb switch, would be similar in form to the model that was obtained for the tunnel-diode switch.

Certainly, any switch that can be expressed in terms of an instantaneous negative-resistance characteristic, a single inductor or capacitor, and a wideband noise source will have the same type of model as the tunnel diode. The same form of switching equation will result and the same relations between the distributions and circuit parameters will exist.

Thus we might expect that a neon-bulb switch or a unijunction transistor will have models of the same form as was obtained for the tunnel diode. These switches probably have a single dynamic element and are probably afflicted by wideband thermal or shot noise. These devices are duals of the tunnel diode, in that their i-v characteristics are current rather than voltage-controlled.

It is not clear a priori whether the model will be the same for more complex multi-device regenerative switching circuits such as the Schmidt-trigger, flip-flop, or PNPN switches. These circuits involve more than one dynamic element, and have noise sources at several locations in the circuit. We have not been able to reduce the small-signal models for these circuits to any simple circuit as we did for the tunnel diode. Experimental observations of the jitter would be useful at this point for obtaining more insight into the switching processes in these circuits.

6.4 QUESTIONS REMAINING ON TUNNEL-DIODE SWITCHING RANDOMNESS

There are many questions still to be answered concerning randomness occurring in tunnel-diode switches. We have only been able to analyze the tunnel-diode jitter model for values of the dimensionless noise spectral height, N_o', in the range $0 \leqslant N_o' < 2$. Since (refer to Eq. 17)

$$N_o' = \frac{kN_o}{C^2 a},\qquad(39)$$

where N_o is the dimensional spectral height of the noise, this region of solution corresponds to analysis when the slope a is not too small. An interesting question therefore concerns the jitter when the slope is very small, or equivalently, when N_o' is very large. We expect that the linear relations (21) obtained in Section IV, may not hold in this small-slope situation.

We have shown that the jitter distribution is a form that satisfies the diffusion equation. It would be interesting to see if this equation might be derived directly from the switching model, thereby by-passing the involved procedure required to solve the "switching equation."

6.5 QUESTIONS REMAINING ON THE GENERAL SWITCHING PROBLEM

Perhaps the most exciting questions concern the modeling of jitter in devices and circuits other than the tunnel diode. An extremely valuable contribution can be made by discovering a procedure whereby switching randomness can be modeled in any of the many types of electronic switches. Some conjectures have been made here concerning

behavior that might be expected in these switches and approaches to the modeling of jitter that might be fruitful.

An interesting group of questions that are very pertinent to switching applications will arise once the general jitter mechanism is determined. These questions involve the optimization of device and circuit configurations to minimize the effects of switching randomness in particular applications. Thus low-jitter circuits might be obtained and procedures for minimizing jitter in a given circuit configuration established. Questions analogous to these were answered for linear amplifiers soon after the small-signal noise models for the circuit components comprising the amplifier were obtained.

APPENDIX A

Schematics of Circuits Used for Measuring the Jitter Statistics

Circuit diagrams for systems used in measuring the statistics of the switching randomness are presented here. Two basic measuring procedures (called "Methods I and II") have been described in Section III. Block diagrams illustrating these procedures are shown in Figs. 7 and 9.

A.1 RAMP GENERATOR AND TUNNEL-DIODE SWITCHES

The schematic in Fig. 27 shows the circuit that was used for generating the ramp, and the pair of diode switches that were triggered by the ramp.

Typical component values:

R_L = 4 kΩ
R_s = 200 Ω
C_s = 0.03 - 20 mf
E = 6 volts

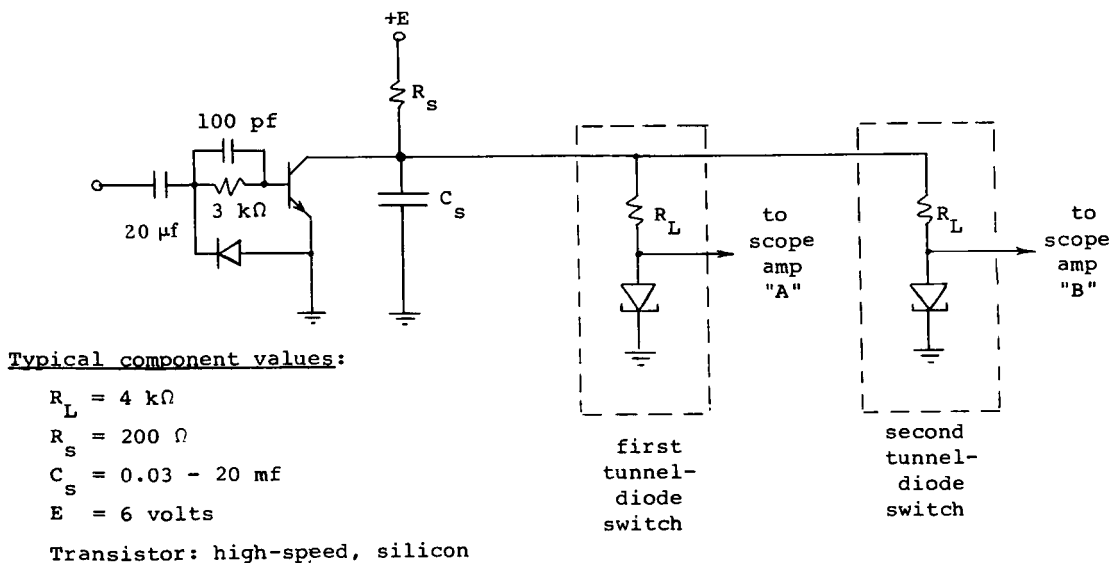Transistor: high-speed, silicon

Fig. 27. Ramp generator and tunnel-diode switches.

While the ramp is forming, the transistor is cut off. Thus practically no shot noise is introduced by the transistor. The only noise in the circuit is thermal noise occurring in R_s and R_L. The effect of these noise sources was shown to be negligible as compared with the shot noise introduced by the diode itself.

The two tunnel-diode switches were shielded from each other. Since no detectable locking or interaction between the two switches could be induced, it is reasonable to assume that they switch independently.

A.2 DIFFERENTIAL TIME-TO-HEIGHT CONVERTER

The differential time-to-height converter is shown in Fig. 28. The outputs from the two diode switches were applied to the "A" and "B" vertical amplifier of a
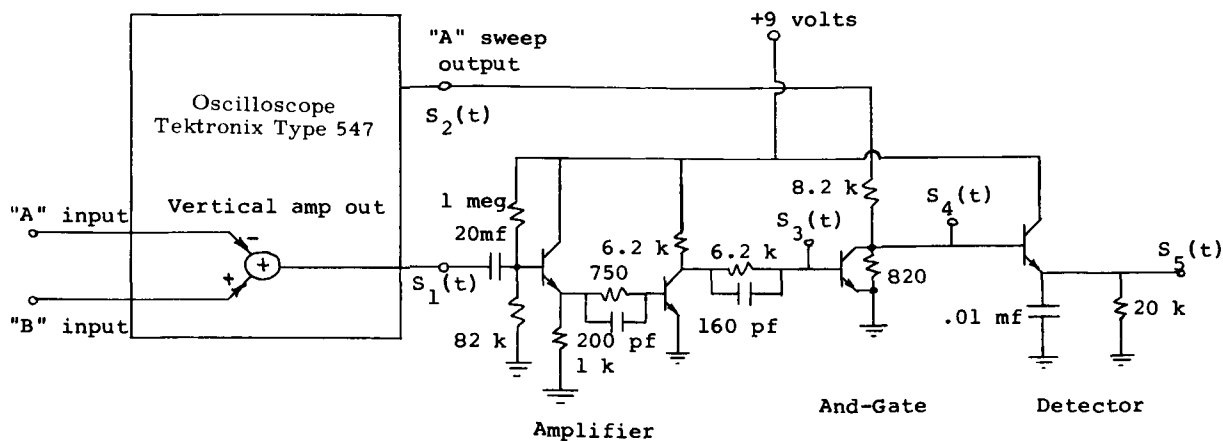
Fig. 28. Differential time-to-height converter.

Techtronix Type 547 oscilloscope, as shown in Fig. 28. One of the two signals was inverted and then added to the other. The waveform $S_1(t)$, shown in Fig. 29, results.

This waveform is amplified and then used to gate the linear horizontal sweep ramp obtained from the oscilloscope. This linear ramp is shown as $S_2(t)$ in Fig. 29. The output, $S_4(t)$, of the and-gate is a pulse with height proportional to the width of the pulse $S_1(t)$. The pulse $S_4(t)$ is passed through a peak-detecting circuit, producing the waveform $S_5(t)$. This last operation was performed in order to give the pulse a much larger area, or energy, thereby producing a much larger signal-to-noise ratio for the measurement.

A.3 FILTER FOR SAMPLING THE CONTINUOUS SPECTRUM $S_r(f)$

Several different types of filters were used for "sampling" the magnitude of $S_r(f)$ (which is proportional to the desired variance of the switching time). (The spectrum $S_r(f)$ has been defined in the description of Method II.) The use of the filter is indicated in the block diagram of Fig. 9 and has already been described.

Two filters were used at various times: (i) A five-pole R-C filter. Five single-pole R-C filters were cascaded with transistor emitter followers between them. The emitter followers provide isolation between the stages of the filter. Extremely high stability, which is necessary for repeatability of the experiments, was obtained by using this brute-force technique. The schematic of this circuit is shown in Fig. 30. (ii) A General
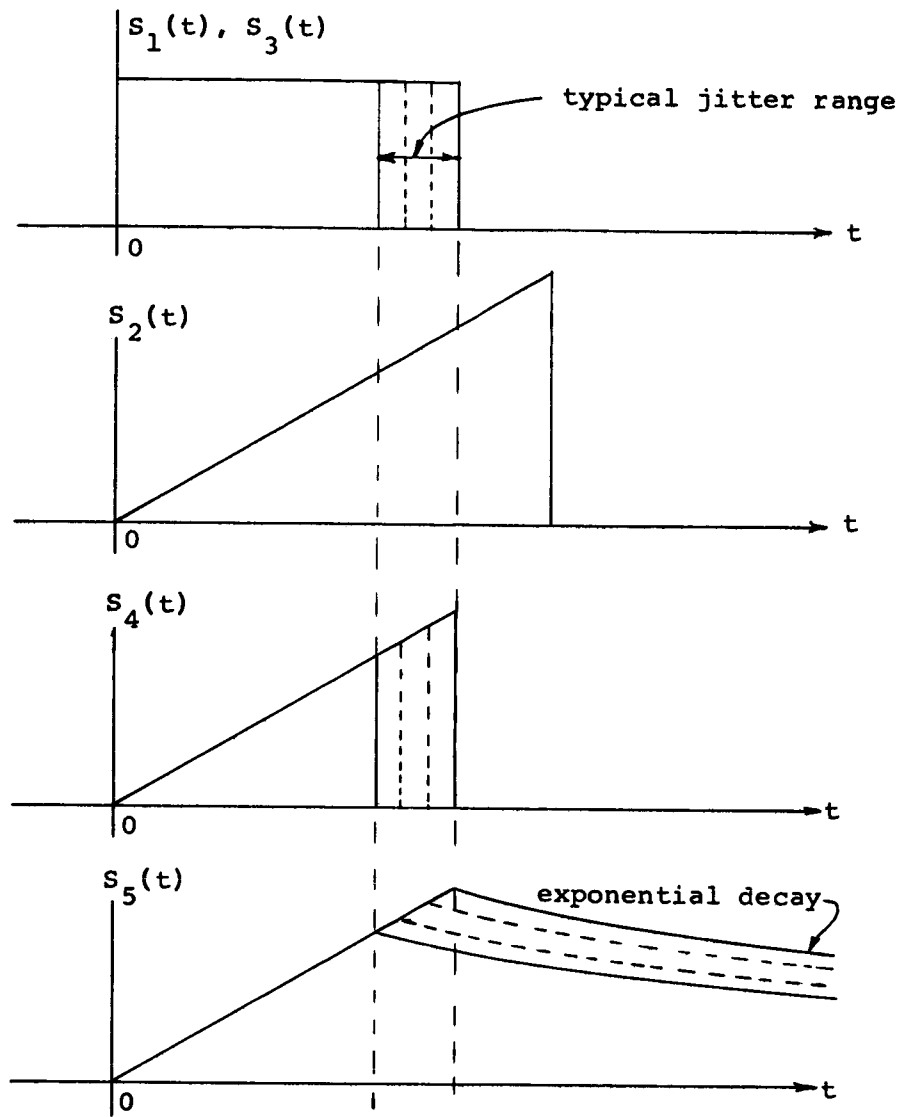
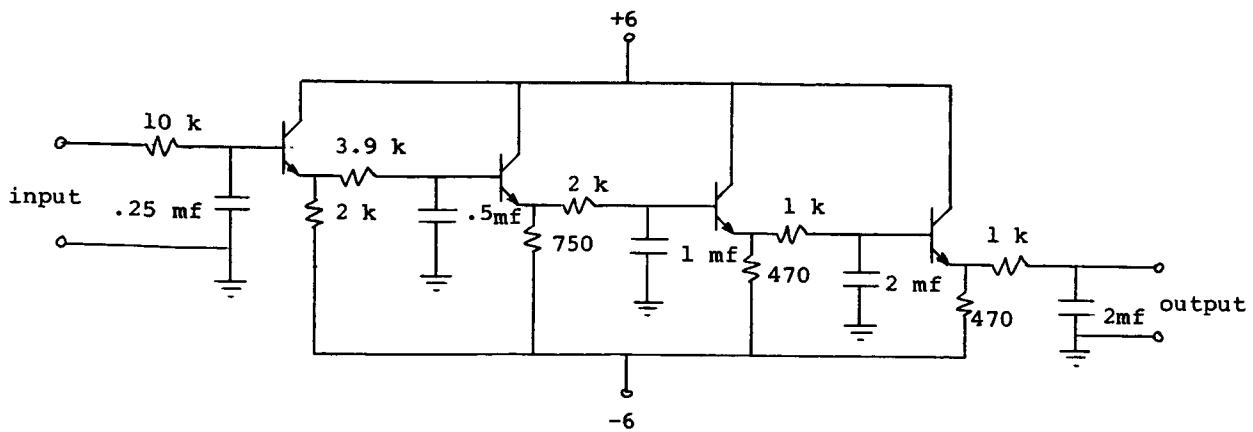Fig. 29. Waveforms obtained in time-to-height converter.

Fig. 30. Stable five-pole lowpass filter used in measurement Method II.

47

Radio Model 1900-A Spectrum Analyzer. This filter was useful for prelimi-
nary tests because of its flexibility.

Power Density Spectrum of the Random Pulse Train of Figure III-4a

The power density spectrum of the random pulse train, f(t), shown in Fig. 8a, will now be computed. A property of the spectrum of this wave was used in the measurement procedure discussed in Section III.

The random signal f(t) can be expressed analytically as

$$f(t) = \sum_{k=-\infty}^{+\infty} x_k h(t-kT), \tag{B.1}$$

where

$$h(t) = e^{-t/\tau} u_{-1}(t). \tag{B.2}$$

The variables x_k are a sequence of statistically independent, identically distributed random variables. The mean and standard deviation of these variables are denoted m_x and σ_x, respectively. The spacing between the pulses is T. The time constant of the exponential is τ.

The power spectrum S(f) of the random wave f(t) has been obtained by others.[7] It can be expressed in the form

$$S(f) = \frac{1}{T} |H(f)|^2 \left[\sigma_x^2 + \frac{m_x^2}{T} \sum_{k=-\infty}^{+\infty} u_0\left(f - \frac{k}{T}\right) \right], \tag{B.3}$$

where H(f) is the Fourier transform of h(t), and $u_0(f)$ is the unit impulse.

The transform of h(t) is

$$H(f) = \frac{\tau}{1 + j2\pi f\tau}. \tag{B.4}$$

By using (B.4), S(f) can be written

$$S(f) = \frac{\tau^2}{1 + (2\pi f\tau)^2} \left[\frac{\sigma_x^2}{T} + \frac{m_x^2}{T^2} \sum_{k=-\infty}^{+\infty} u_0\left(f - \frac{k}{T}\right) \right]. \tag{B.5}$$

Observe that S(f) can be expressed in the form

$$S(f) = S_r(f) + S_p(f), \tag{B.6}$$

where $S_p(f)$ contains only impulses at harmonics of the frequency $1/T$, and $S_r(f)$ is

continuous. The impulsive component $S_p(f)$ is due to the periodic part of $f(t)$. These two components are

$$S_p(f) = \frac{m_x^2 \tau^2}{T^2} \frac{1}{1 + (2\pi f\tau)^2} \sum_{k=-\infty}^{+\infty} u_o\left(f - \frac{k}{T}\right)$$ (B.7)

and

$$S_r(f) = \frac{\sigma_x^2 \tau^2}{T} \frac{1}{1 + (2\pi f\tau)^2}.$$ (B.8)

The property that $S_r(f)$ is proportional to the variance σ_x^2 was used in experimentally determining the variance of the switching times.

APPENDIX C

Computer Solution of the Switching Equation

The program used for solving the switching equation derived in Section IV will now be presented and discussed. The switching equation in dimensionless form is

$$\frac{dv}{dt} - v^2 = t + n(t), \qquad (C.1)$$

where $n(t)$ is white noise with spectral height N_o. The primes that were used with the dimensionless variables in Section IV are omitted here.

C.1 GENERAL CHARACTERISTICS OF THE SWITCHING EQUATION

A property of Eq. C.1 is that if its right side is negative and if the initial value of v is negative, then $v(t)$ will tend to some stable finite value. On the other hand, if the right side is positive, $v(t)$ will tend to infinity within some finite time. We shall consider this time to be the "switching time," and denote it T_s.

For a given set of initial conditions and $n(t) = 0$, the switching will always occur at the same time. When noise is added, however, T_s becomes a random variable, taking on values distributed about some mean. The distribution of T_s will depend on the amount of noise present, that is, on N_o, and on the initial starting voltage and time.

The initial voltage, v_o, and time, t_o, are chosen so that the system would effectively
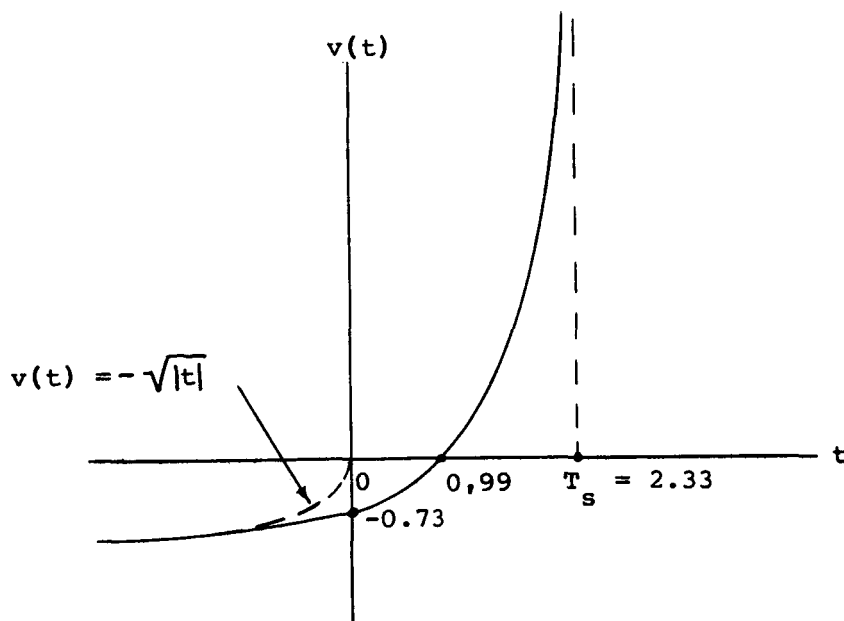

Fig. 31. Solution of the dimensionless switching equation with $n(t) = 0$, obtained by computer.

have been in equilibrium at large negative times. This condition is ensured if

$$v_o = - \sqrt{|t_o|},$$ (C.2)

where t_o, the initial starting time, is a large negative number. With this restriction, the operating point will follow the i-v relation, $i(v) = -kv^2$, until the region of switching is reached. The solution for these conditions and for $n(t) = 0$ is shown in Fig. 31.

C.2 COMPUTER SOLUTION OF THE SWITCHING EQUATION

The object of the computation was to obtain the distribution, mean, and standard deviation of the switching time. The computation was performed on an IBM 7094 computer using the Fortran II language.

The equation was solved for $v(t)$ by using standard one-step difference techniques. Noise was introduced by adding in a random number at each iteration of the difference equation. The random-number sequence was obtained by using the "RANNOF" routine. This routine generates a pseudo-random sequence of numbers that are uniformly distributed between zero and one, and which, for our purpose, can be considered to be mutually independent. The sequence was adjusted to have zero mean and a variance corresponding to a given spectral height, N_o.

The solution was started far enough back in time, subject to the initial condition (A3.2), to ensure that the process would appear to have been going indefinitely. When $v(t)$ became large enough to ensure that the noise would have negligible effect on the future course of the signal, the computation was stopped, and the final values of v and t were substituted into an asymptotic solution that is valid for large v. From this asymptotic form the switching time T_s was obtained.

N_o was set to some specified value and this solution procedure was carried out 1000 times, resulting in that many values of the random variable T_s. By using standard computing techniques, the mean, standard deviation, and distribution of T_s were calculated. These statistics were obtained for values of N_o ranging from zero up to four.

C.3 PROGRAM FOR SOLVING THE SWITCHING EQUATION

Some of the special features of the program that was used for computing the solution of the switching equation will now be discussed. The program, written in the Fortran II language, is shown below.

The input variables are defined as follows:

VO = initial voltage, v_o.

TO = initial time, t_o.

SO = spectral height of the noise, N_o.

DELTA = size of time increments, or steps.

52

```
      DIMENSION TS(1000)
      READ 10, L
 10 FORMAT (I2)
      READ 1, VO,TO,DELTA,SO,M
  1 FORMAT (2F10.4, F10.7, F10.4,I10)
      PRINT 2 , VO,TO,DELTA,SO,M
  2 FORMAT (1H1,//,5HVO = ,F10.4,4X4HTO = ,F10.4,
   14X7HDELTA = ,F10.7,4X4HSO = ,F10.4,4X4HM = ,I4)
      PRINT 11, L
 11 FORMAT (7HOSETUF( , I2,1H))
      PRINT 8
  8 FORMAT (16HOSWITCHING TIMES)
      B = SETUF(L)
      DO 12 I=1, 50
 12 Z = RANNOF(X)
      A = SQRTF(12.*DELTA*SO)
      DELSQ = .5*DELTA*DELTA
      DO 13 I=1,M
      DO 5 J = 1,5
      V = VO
      DO 4 N=1,10000
      Z = RANNOF(X)
      T = TO+DELTA*FLOATF(N)
      V=V/(1.-DELTA*V)+DELTA*T+DELSQ+A*(Z-.5)
      IF (V-30.) 4,5,5
  4 CONTINUE
  5 TS(J) = T+1./V
      PRINT 6, (TS(J), J=1,5)
  6 FORMAT (5F12.6)
 13 PUNCH 6, (TS(J), J=1,5)
      CALL EXIT
      END
*     DATA
```

M = number of output cards desired. Five values of the switching time are , punched on each card. We usually solved for 1000 values of T_s, corresponding to M = 200.

With these inputs specified, the program would solve for 5M values of the switching time, T_s. These values would be punched onto cards as well as printed.

Standard programs (not included) were used to compute the distribution, mean, and standard deviation of the computed values of T_s.

a. Asymptotic Form of the Switching Equation and Its Use

The switching equation can be written in the form

$$\frac{dv}{dt} = v^2 + t + n(t).$$ (C.3)

When v becomes large, this equation has the asymptotic form,

$$\frac{dv}{dt} = v^2.$$ (C.4)

The solution of this equation, easily found by integration, is

$$v(t) = \frac{1}{T_s - t}.$$ (C.5)

When v(t) begins to blow up as it approaches the singularity at $t = T_s$, the computation becomes very inaccurate. To avoid this problem, we stopped the computation at the first value of v that exceeded 30. These final values of voltage and time, v_f and t_f, respectively, were then substituted in the asymptotic solution (C.5), to yield the desired switching time,

$$T_s = t_f + \frac{1}{v_f}.$$ (C.6)

Acknowledgement

References

1. C. N. Berglund, "An Experimental Investigation of Noise in Tunnel Diodes," Report ESL-R-115, Electronics Systems Laboratory, Massachusetts Institute of Technology, Cambridge, Mass., July 1961.

2. R. A. Pucel, "The Equivalent Noise Current of Esaki Diodes," Proc. IRE 49, 49 (1961).

3. B. E. Turner and R. E. Burgess, "Direct Tunnel-Current Noise in Tunnel Diodes for Small Biases," Can. J. Phys. 42, 1046 (June 1964).

4. Yajima and Esaki, "Excess Noise in Narrow p-n Junctions," J. Phys. Soc. Japan 13, 1281 (1958).

5. H. Cramér, Random Variables and Probability Distributions (Cambridge University Press, London, 1937), p. 53, Theorem 19.

6. H. Davis, Introduction to Non-linear Differential Equations (Dover Publications Inc., New York, 1962), pp. 3-8; 57-58.

7. J. L. Lawson and G. E. Uhlenbeck, Threshold Signals (McGraw-Hill Book Company, New York, 1950), pp. 43-44.

JOINT SERVICES ELECTRONICS PROGRAM
REPORTS DISTRIBUTION LIST

Department of Defense

Dr. Edward M. Reilley
Asst Director (Research)
Ofc of Defense Res & Eng
Department of Defense
Washington, D.C. 20301

Office of Deputy Director
(Research and Information Room 3D1037)
Department of Defense
The Pentagon
Washington, D.C. 20301

Director
Advanced Research Projects Agency
Department of Defense
Washington, D.C. 20301

Director for Materials Sciences
Advanced Research Projects Agency
Department of Defense
Washington, D.C. 20301

Headquarters
Defense Communications Agency (333)
The Pentagon
Washington, D.C. 20305

Defense Documentation Center
Attn: TISIA
Cameron Station, Bldg. 5
Alexandria, Virginia 22314

Director
National Security Agency
Attn: Librarian C-332
Fort George G. Meade, Maryland 20755

Weapons Systems Evaluation Group
Attn: Col. Daniel W. McElwee
Department of Defense
Washington, D.C. 20305

National Security Agency
Attn: R4-James Tippet
        Office of Research
Fort George G. Meade, Maryland 20755

Central Intelligence Agency
Attn: OCR/DD Publications
Washington, D.C. 20505

Department of the Air Force

Colonel Kee
AFRSTE
Hqs. USAF
Room ID-429, The Pentagon
Washington, D.C. 20330

AMD (AMRXI)
Brooks AFB, Texas 78235

AUL3T-9663
Maxwell AFB, Alabama 36112

AFFTC (FTBPP-2)
Technical Library
Edwards AFB, Calif. 93523

SAMSO (SMSDI-STINFO)
AF Unit Post Office
Los Angeles
California 90045

Major Charles Waespy
Technical Division
Deputy for Technology
Space Systems Division, AFSC
Los Angeles, California 90045

SSD(SSTRT/Lt. Starbuck)
AFUPO
Los Angeles, California 90045

Det #6, OAR (LOOAR)
Air Force Unit Post Office
Los Angeles, California 90045

ARL (ARIY)
Wright-Patterson AFB, Ohio 45433

Dr. H. V. Noble
Air Force Avionics Laboratory
Wright-Patterson AFB, Ohio 45433

Mr. Peter Murray
Air Force Avionics Laboratory
Wright-Patterson AFB, Ohio 45433

AFAL (AVTE/R. D. Larson)
Wright-Patterson AFB, Ohio 45433

Commanding General
Attn: STEWS-WS-VT
White Sands Missile Range
New Mexico 88002

RADC (EMLAL-1)
Griffiss AFB, New York 13442
Attn: Documents Library

Academy Library (DFSLB)
U.S. Air Force Academy
Colorado Springs, Colorado 80912

Lt. Col. Bernard S. Morgan
Frank J. Seiler Research Laboratory
U.S. Air Force Academy
Colorado Springs, Colorado 80912

APGC (PGBPS-12)
Eglin AFB, Florida 32542

AFETR Technical Library
(ETV, MU-135)
Patrick AFB, Florida 32925

AFETR (ETLLG-1)
STINFO Officer (for Library)
Patrick AFB, Florida 32925

Dr. L. M. Hollingsworth
AFCRL (CRN)
L. G. Hanscom Field
Bedford, Massachusetts 01731

AFCRL (CRMXLR)
AFCRL Research Library, Stop 29
L. G. Hanscom Field
Bedford, Massachusetts 01731

Colonel Robert E. Fontana
Department of Electrical Engineering
Air Force Institute of Technology
Wright-Patterson AFB, Ohio 45433

Colonel A. D. Blue
RTD (RTTL)
Bolling Air Force Base, D.C. 20332

Dr. I. R. Mirman
AFSC (SCT)
Andrews Air Force Base, Maryland 20331

Colonel J. D. Warthman
AFSC (SCTR)
Andrews Air Force Base, Maryland 20331

Lt. Col. J. L. Reeves
AFSC (SCBB)
Andrews Air Force Base, Maryland 20331

ESD (ESTI)
L. G. Hanscom Field
Bedford, Massachusetts 01731

AEDC (ARO, INC)
Attn: Library/Documents
Arnold AFS, Tennessee 37389

European Office of Aerospace Research
Shell Building
47 Rue Cantersteen
Brussels, Belgium

Lt. Col. Robert B. Kalisch
Chief, Electronics Division
Directorate of Engineering Sciences
Air Force Office of Scientific Research
Arlington, Virginia 22209

Department of the Army

U.S. Army Research Office
Attn: Physical Sciences Division
3045 Columbia Pike
Arlington, Virginia 22204

Research Plans Office
U.S. Army Research Office
3045 Columbia Pike
Arlington, Virginia 22204

Commanding General
U.S. Army Materiel Command
Attn: AMCRD-RS-DE-E
Washington, D.C. 20315

Commanding General
U.S. Army Strategic Communications
    Command
Washington, D.C. 20315

Commanding Officer
U.S. Army Materials Research Agency
Watertown Arsenal
Watertown, Massachusetts 02172

Commanding Officer
U.S. Army Ballistics Research Laboratory
Attn: V. W. Richards
Aberdeen Proving Ground
Aberdeen, Maryland 21005

Commandant
U.S. Army Air Defense School
Attn: Missile Sciences Division C&S Dept.
P.O. Box 9390
Fort Bliss, Texas 79916

Commanding General
U.S. Army Missile Command
Attn: Technical Library
Redstone Arsenal, Alabama 35809

Commanding General
Frankford Arsenal
Attn: L600-64-4 (Dr. Sidney Ross)
Philadelphia, Pennsylvania 19137

U.S. Army Munitions Command
Attn: Technical Information Branch
Picatinney Arsenal
Dover, New Jersey 07801

Commanding Officer
Harry Diamond Laboratories
Attn: Dr. Berthold Altman (AMXDO-TI)
Connecticut Avenue and Van Ness St. N. W.
Washington, D.C. 20438

Commanding Officer
U.S. Army Security Agency
Arlington Hall
Arlington, Virginia 22212

Commanding Officer
U.S. Army Limited War Laboratory
Attn: Technical Director
Aberdeen Proving Ground
Aberdeen, Maryland 21005

Commanding Officer
Human Engineering Laboratories
Aberdeen Proving Ground, Maryland 21005

Director
U.S. Army Engineer
Geodesy, Intelligence and Mapping
Research and Development Agency
Fort Belvoir, Virginia 22060

Commandant
U.S. Army Command and General
    Staff College
Attn: Secretary
Fort Leavenworth, Kansas 66270

Dr. H. Robl, Deputy Chief Scientist
U.S. Army Research Office (Durham)
Box CM, Duke Station
Durham, North Carolina 27706

Commanding Officer
U.S. Army Research Office (Durham)
Attn: CRD-AA-IP (Richard O. Ulsh)
Box CM, Duke Station
Durham, North Carolina 27706

Librarian
U.S. Army Military Academy
West Point, New York 10996

The Walter Reed Institute of Research
Walter Reed Medical Center
Washington, D.C. 20012

Commanding Officer
U.S. Army Engineer R&D Laboratory
Attn: STINFO Branch
Fort Belvoir, Virginia 22060

Commanding Officer
U.S. Army Electronics R&D Activity
White Sands Missile Range,
    New Mexico 88002

Dr. S. Benedict Levin, Director
Institute for Exploratory Research
U.S. Army Electronics Command
Fort Monmouth, New Jersey 07703

Director
Institute for Exploratory Research
U.S. Army Electronics Command
Attn: Mr. Robert O. Parker, Executive
    Secretary, JSTAC (AMSEL-XL-D)
Fort Monmouth, New Jersey 07703

Commanding General
U.S. Army Electronics Command
Fort Monmouth, New Jersey 07703
Attn:

AMSEL-SC	HL-CT-A
RD-D	NL-D
RD-G	NL-A
RD-GF	NL-P
RD-MAT	NL-R
XL-D	NL-S
XL-E	KL-D
XL-C	KL-E
XL-S	KL-S
HL-D	KL-TM
HL-CT-R	KL-TQ
HL-CT-P	KL-TS
HL-CT-L	VL-D
HL-CT-O	WL-D
HL-CT-I	

Department of the Navy

Chief of Naval Research
Department of the Navy
Washington, D.C. 20360
Attn: Code 427

Naval Electronics Systems Command
ELEX 03
Falls Church, Virginia 22046

Naval Ship Systems Command
SHIP 031
Washington, D.C. 20360

Naval Ship Systems Command
SHIP 035
Washington, D.C. 20360

Naval Ordnance Systems Command
ORD 32
Washington, D.C. 20360

Naval Air Systems Command
AIR 03
Washington, D.C. 20360

Commanding Officer
Office of Naval Research Branch Office
Box 39, Navy No 100 F.P.O.
New York, New York 09510

Commanding Officer
Office of Naval Research Branch Office
219 South Dearborn Street
Chicago, Illinois 60604

Commanding Officer
Office of Naval Reasearch Branch Office
1030 East Green Street
Pasadena, California 91101

Commanding Officer
Office of Naval Research Branch Office
207 West 24th Street
New York, New York 10011

Commanding Officer
Office of Naval Research Branch Office
495 Summer Street
Boston, Massachusetts 02210

Director, Naval Research Laboratory
Technical Information Officer
Washington, D.C. 20360
Attn: Code 2000

Commander
Naval Air Development and Material Center
Johnsville, Pennsylvania 18974

Librarian
U.S. Naval Electronics Laboratory
San Diego, California 95152

Commanding Officer and Director
U.S. Naval Underwater Sound Laboratory
Fort Trumbull
New London, Connecticut 06840

Librarian
U.S. Navy Post Graduate School
Monterey, California 93940

Commander
U.S. Naval Air Missile Test Center
Point Magu, California 93041

Director
U.S. Naval Observatory
Washington, D.C. 20390

Chief of Naval Operations
OP-07
Washington, D.C. 20350

Director, U.S. Naval Security Group
Attn: G43
3801 Nebraska Avenue
Washington, D.C. 20390

Commanding Officer
Naval Ordnance Laboratory
White Oak, Maryland 21502

Commanding Officer
Naval Ordnance Laboratory
Corona, California 91720

Commanding Officer
Naval Ordnance Test Station
China Lake, California 93555

Commanding Officer
Naval Avionics Facility
Indianapolis, Indiana 46241

Commanding Officer
Naval Training Device Center
Orlando, Florida 32811

U.S. Naval Weapons Laboratory
Dahlgren, Virginia 22448

Weapons Systems Test Division
Naval Air Test Center
Patuxtent River, Maryland 20670
Attn: Library

Head, Technical Division
U.S. Naval Counter Intelligence
    Support Center
Fairmont Building
4420 North Fairfax Drive
Arlington, Virginia 22203

Other Government Agencies

Mr. Charles F. Yost
Special Assistant to the Director
    of Research
National Aeronautics and
    Space Administration
Washington, D.C. 20546

Dr. H. Harrison, Code RRE
Chief, Electrophysics Branch
National Aeronautics and
    Space Administration
Washington, D.C. 20546

Goddard Space Flight Center
National Aeronautics and
    Space Administration
Attn: Library C3/TDL
Green Belt, Maryland 20771

NASA Lewis Research Center
Attn: Library
21000 Brookpark Road
Cleveland, Ohio 44135

National Science Foundation
Attn: Dr. John R. Lehmann
Division of Engineering
1800 G Street, N.W.
Washington, D.C. 20550

U.S. Atomic Energy Commission
Division of Technical Information Extension
P.O. Box 62
Oak Ridge, Tennessee 37831

Los Alamos Scientific Laboratory
Attn: Reports Library
P.O. Box 1663
Los Alamos, New Mexico 87544

NASA Scientific & Technical Information
    Facility
Attn: Acquisitions Branch (S/AK/DL)
P.O. Box 33,
College Park, Maryland 20740

NASA, Langley Research Center
Langley Station
Hampton, Virginia 23365
Attn: Mr. R. V. Hess, Mail Stop 160

Non-Government Agencies

Director
Research Laboratory of Electronics
Massachusetts Institute of Technology
Cambridge, Massachusetts 02139

Polytechnic Institute of Brooklyn
55 Johnson Street
Brooklyn, New York 11201
Attn: Mr. Jerome Fox
       Research Coordinator

Director
Columbia Radiation Laboratory
Columbia University
538 West 120th Street
New York, New York 10027

Director
Coordinated Science Laboratory
University of Illinois
Urbana, Illinois 61803

Director
Stanford Electronics Laboratories
Stanford University
Stanford, California 94305

Director
Electronics Research Laboratory
University of California
Berkeley, California 94720

Director
Electronic Sciences Laboratory
University of Southern California
Los Angeles, California 90007

Professor A. A. Dougal, Director
Laboratories for Electronics and
       Related Sciences Research
University of Texas
Austin, Texas 78712

Gordon McKay Library A175
Technical Reports Collection
Harvard College
Cambridge, Massachusetts 02138

Aerospace Corporation
P.O. Box 95085
Los Angeles, California 90045
Attn: Library Acquisitions Group

Professor Nicholas George
California Institute of Technology
Pasadena, California 91109

Aeronautics Library
Graduate Aeronautical Laboratories
California Institute of Technology
1201 E. California Blvd.
Pasadena, California 91109

Director, USAF Project RAND
Via: Air Force Liaison Office
The RAND Corporation
1700 Main Street
Santa Monica, California 90406
Attn: Library

The Johns Hopkins University
Applied Physics Laboratory
8621 Georgia Avenue
Silver Spring, Maryland 20910
Attn: Boris W. Kuvshinoff
Document Librarian

Hunt Library
Carnegie Institute of Technology
Schenley Park
Pittsburgh, Pennsylvania 15213

Dr. Leo Young
Stanford Research Institute
Menlo Park, California 94025

Mr. Henry L. Bachmann
Assistant Chief Engineer
Wheeler Laboratories
122 Cuttermill Road
Great Neck, New York 11021

School of Engineering Sciences
Arizona State University
Tempe, Arizona 85281

Engineering and Mathematical
Sciences Library
University of California
405 Hilgrad Avenue
Los Angeles, California 90024

California Institute of Technology
Pasadena, California 91109
Attn: Documents Library

University of California
Santa Barbara, California 93106
Attn: Library

Carnegie Institute of Technology
Electrical Engineering Department
Pittsburgh, Pennsylvania 15213

University of Michigan
Electrical Engineering Department
Ann Arbor, Michigan 48104

New York University
College of Engineering
New York, New York 10019

Syracuse University
Dept. of Electrical Engineering
Syracuse, New York 13210

Yale University
Engineering Department
New Haven, Connecticut 06520

Airborne Instruments Laboratory
Deerpark, New York 11729

Bendix Pacific Division
11600 Sherman Way
North Hollywood, California 91605

General Electric Company
Research Laboratories
Schenectady, New York 12301

Lockheed Aircraft Corporation
P.O. Box 504
Sunnyvale, California 94088

Raytheon Company
Bedford, Massachusetts 01730
Attn: Librarian

Dr. G. J. Murphy
The Technological Institute
Northwestern University
Evanston, Illinois 60201

Dr. John C. Hancock, Director
Electronic Systems Research Laboratory
Purdue University
Lafayette, Indiana 47907

Director
Microwave Laboratory
Stanford University
Stanford, California 94305

Emil Schafer, Head
Electronics Properties Info Center
Hughes Aircraft Company
Culver City, California 90230

Department of Electrical Engineering
Texas Technological College
Lubbock, Texas 79409

DOCUMENT CONTROL DATA - R & D

(Security classification of title, body of abstract and indexing annotation must be entered when the overall report is classified)

1. ORIGINATING ACTIVITY (Corporate author)	2a. REPORT SECURITY CLASSIFICATION
Research Laboratory of Electronics Massachusetts Institute of Technology Cambridge, Massachusetts 02139	Unclassified
	2b. GROUP None

3. REPORT TITLE

Statistics of Switching-Time Jitter for a Tunnel Diode Threshold-Crossing Detector

4. DESCRIPTIVE NOTES (Type of report and inclusive dates)

Technical Report

5. AUTHOR(S) (First name, middle initial, last name)

Donald E. Nelsen

6. REPORT DATE August 31, 1967	7a. TOTAL NO. OF PAGES 72	7b. NO. OF REFS. 7
8a. CONTRACT OR GRANT NO. DA 28-043-AMC-02536(E) b. PROJECT NO. 200-14501-B31F c. NASA Grant NsG-496 d.	9a. ORIGINATOR'S REPORT NUMBER(S) Technical Report 456	
	9b. OTHER REPORT NO(S) (Any other numbers that may be assigned this report) None	

10. DISTRIBUTION STATEMENT

Distribution of this report is unlimited

11. SUPPLEMENTARY NOTES	12. SPONSORING MILITARY ACTIVITY Joint Services Electronics Program thru USAECOM, Fort Monmouth, N. J.

13. ABSTRACT

As a step toward obtaining a procedure for modeling randomness occurring in electronic switching circuits, the switching randomness, or jitter, arising in a tunnel-diode switch was investigated. Distributions of the switching time were measured for a tunnel-diode switching circuit that was driven by a slowly rising current ramp. A model was deduced from these measurements which relates the statistics of the jitter to the slope of the input ramp, the load resistance, and the tunnel-diode characteristics in the vicinity of the current peak: the amount of shot noise, junction capacitance, and i-v relation curvature. For switching in the reverse direction — from the valley of the i-v relation back to the initial state — the switching randomness involves a different mechanism. Another model is presented for this case. This model relates the jitter to the 1/f noise that predominates in the valley region of the tunnel diode.

DD FORM 1473 1 NOV 65

14. KEY WORDS	LINK A		LINK B		LINK C	
	ROLE	WT	ROLE	WT	ROLE	WT
Jitter in Electronic Switches						
Tunnel-Diode Switch, jitter in						
Switching Time, jitter of						
Switching Circuits, jitter in						
Switching-Time Randomness						
Random Processes in Tunnel-Diode Switch						